Title

A paleotemperature record derived from dissolved noble gases in groundwater of the Aquia Aquifer (Maryland, USA)

Journal

Geochimica et Cosmochimica Acta, 66(5)

ISSN

0016-7037

Authors

Aeschbach-Hertig, Werner
Stute, Martin
Clark, Jordan F
et al.

Publication Date

2002-03-01

DOI

10.1016/s0016-7037(01)00804-3

Peer reviewed

Pergamon

Geochimica et Cosmochimica Acta, Vol. 66, No. 5, pp. 797–817, 2002

0016-7037/02 $22.00 + .00

PII S0016-7037(01)00804-3

A paleotemperature record derived from dissolved noble gases in groundwater of the Aquia Aquifer (Maryland, USA)

WERNER AESCHBACH-HERTIG,[1,2,*] MARTIN STUTE,[1,3] JORDAN F. CLARK,[4] ROBERT F. REUTER,[5] and PETER SCHLOSSER[1,6]

[1]Lamont-Doherty Earth Observatory of Columbia University, Palisades, New York, USA
[2]now at Swiss Federal Institute of Technology (ETH), Zurich, and Swiss Federal Institute of Environmental Science and Technology (EAWAG), Dübendorf. Switzerland
[3]Department of Environmental Science, Barnard College, New York, USA
[4]University of California at Santa Barbara, Santa Barbara, California, USA
[5]Chemistry and Biochemistry Department, University of Maryland, College Park, Maryland, USA
[6]Department of Earth and Environmental Engineering, Columbia University, New York, USA

(*Received March* 29, 2001; *accepted in revised form August* 17, 2001)

Abstract—Low ^{14}C activities in groundwater of the confined part of the Aquia aquifer in southeastern Maryland suggest that most of this water infiltrated at least 30,000 years ago. However, radiocarbon contents of the dissolved inorganic carbon seem to be affected by isotopic exchange, possibly with secondary calcite deposits in the formation, leading to overestimated ^{14}C ages. Whereas the geochemistry of the Aquia aquifer complicates the application of the widely used ^{14}C dating method, the accumulation of radiogenic He seems to provide a viable alternative for establishing a chronology. The quasi-linear increase of He concentrations with flow distance observed in the Aquia aquifer can be explained entirely by accumulation of in situ produced radiogenic He. U and Th concentrations in Aquia sand were measured in order to determine the accumulation rate of ^{4}He with sufficient confidence to establish a He time scale.

Concentrations of dissolved atmospheric noble gases were used to derive mean annual ground temperatures at the time of infiltration. These noble gas temperatures (NGTs) clearly show the presence of water that infiltrated under much cooler conditions than at present. NGTs are correlated with chloride concentrations, corroborating the hypothesis that chloride variations in this aquifer constitute a climate signal. In contrast, the stable isotope ratios $\delta^{18}0$ and δD do not provide a clear record of past climatic changes in the Aquia aquifer and the correlation between NGTs and stable isotope ratios is weak. The NGT record suggests that mean annual temperatures in this midlatitude coastal site during the last glacial maximum (LGM) were (9.0 ± 0.6) °C colder than during the Holocene. This difference is slightly lower than estimates derived from pollen data for this region, but considerably larger than the rather uniform cooling of about 5°C indicated by noble gas studies in more southern locations of North America. The larger cooling is ascribed to the influence of the Laurentide ice sheet, which at its maximum extension came as close as 250 km to our study site.

1. INTRODUCTION

Accurate data about past climate states such as the last glacial maximum (LGM) are a prerequisite for a better understanding of the global climate system. Despite numerous research efforts, our knowledge of the global surface temperatures during the LGM is still incomplete and in part controversial. In the tropics, continental proxies such as snowlines, pollen (Colinvaux et al., 1996), oxygen isotopes in glaciers (Thompson et al., 1995), and noble gases in aquifers (Stute et al., 1995b) indicate that temperatures during the LGM were ~5°C lower than at present. These findings contrast with estimates of at most 2°C cooler tropical sea surface temperatures obtained from species assemblages of foraminifera (CLIMAP, 1976, 1981), although the discrepancy has been somewhat diminished by reassessments of the faunal data (see review by Crowley, 2000). In polar regions, ice-sheet borehole temperatures (Cuffey et al., 1995; Johnsen et al., 1995) indicate a glacial temperature depression of 15 to 20°C, considerably larger than previously inferred from oxygen isotope records (e.g., Johnsen et al., 1992).

Although the exact magnitude of the LGM-Holocene temperature change for both the warmest and coldest regions of the Earth is still being debated, the equator to pole temperature gradient was certainly larger during the LGM than it is today. Climate models indicate that the large ice sheets on the northern continents, and in North America in particular, had a profound effect on the distribution of surface temperatures (Manabe and Broccoli, 1985; COHMAP, 1988; Bartlein et al., 1998). Both models and pollen-based climate reconstructions indicate that sites close to the Laurentide ice sheets experienced a larger LGM-Holocene temperature difference than sites further south, although there are considerable differences between the results of the two approaches (Webb III et al., 1998; Jackson et al., 2000). Independent quantitative paleoclimate reconstructions are desirable to improve our view of the LGM climate in regions influenced by ice sheets.

The "noble gas thermometer" constitutes a quantitative tool to measure local LGM-Holocene temperature changes, because it is based on a simple physical principle, namely the temperature dependence of the solubility of noble gases in water. Concentrations of dissolved noble gases recorded in confined

* Author to whom correspondence should be addressed (aeschbach@eawag.ch).

aquifers reflect the ground temperature during groundwater infiltration (e.g., Stute and Schlosser, 1993, 2000). The situation is complicated by entrapment and dissolution of air during groundwater infiltration, giving rise to an additional, temperature-independent noble gas component, the so-called "excess air" (Heaton and Vogel, 1981). Yet, recent methodologic work (Ballentine and Hall, 1999; Aeschbach-Hertig et al., 1999, 2000) has shown that measured noble gas concentrations in groundwater can consistently be modeled within the analytical uncertainties of typically ± 1 to 2% and that the noble gas temperature (NGT) and its uncertainty can reliably be determined.

A major drawback of the groundwater archive is its inherently low temporal resolution due to dispersive mixing and the difficulty of accurate dating. The reliability of ^{14}C ages is limited by our ability to model the different sources and sinks of dissolved carbon in aquifers. Noble gas studies provide a time indicator, namely radiogenic He, which is produced by α-emitting isotopes of the U and Th radioactive decay series and subsequently accumulated in groundwater. However, uncertainties in the sources and the accumulation rate usually preclude the use of He as a quantitative dating tool.

So far, noble gas studies have provided rather uniform results of $\sim$5°C for the LGM-Holocene temperature change in the tropics and subtropics (for a review see Farrera et al., 1999). Temperature differences of $\sim$5 to 7°C were found in studies at higher latitudes in Europe (e.g., Andrews and Lee, 1979; Andrews et al., 1985; Rudolph et al., 1984; Beyerle et al., 1998). However, in some of these NGT records, the LGM could not be clearly identified, possibly because glaciation or permafrost prevented groundwater recharge during the LGM (Andrews and Lee, 1979; Beyerle et al., 1998). A substantially larger than 5°C LGM-Holocene temperature change ($\geq$8.6°C) was found only in the Great Hungarian Plain (Stute and Sonntag, 1992).

This study presents dissolved noble gas concentrations from the Aquia aquifer in Maryland (USA), and their interpretation in terms of NGTs and radiogenic He accumulation. Favorable conditions in the Aquia aquifer allow us to derive He accumulation ages and thus a purely noble gas based climate record that is complemented by data on groundwater chemistry, stable isotopes, and radiocarbon. The study site at 39°N on the east coast of North America complements records from more southerly locations in North America (Stute et al., 1992a, 1995a; Clark et al., 1997, 1998) to a data set that can be used to discuss the latitudinal temperature gradient during the LGM and the influence of the Laurentide ice sheet on the glacial climate in its vicinity.

2. STUDY AREA

The Aquia formation is a Paleocene layer in the sequence of unconsolidated sediments of the Atlantic Coastal Plain, reaching from Virginia through Delaware, USA. This study is focused on the part of the Aquia located in southern Maryland west of the Chesapeake Bay (Fig. 1). In this region, the Aquia outcrops between Washington D.C. and Annapolis and dips southeast towards the ocean. The groundwater generally flows in a more easterly direction, as indicated by the reconstructed prepumping potentiometric surface (Fig. 1, Chapelle and Drummond, 1983; Chapelle, 1983). In its confined part, the aquifer is an important water resource. Intensive pumping has locally led to strong drawdown of the potentiometric surface. The area investigated in this study was restricted to avoid potential complications due to the most prominent depression cone near Lexington Park (south of point B in Fig. 1).

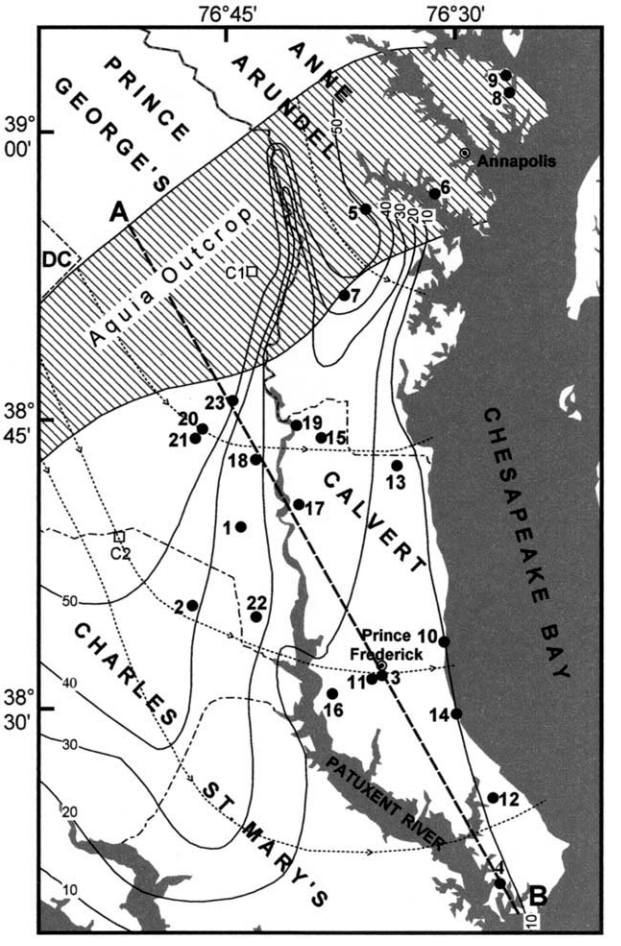

Fig. 1. Map of the study area, with county names and boundaries (dash-dotted) and major cities. Sampled wells are indicated by dots and numbers. The squares C1 and C2 indicate the location of the two sampled sediment cores. Contours of the prepumping potentiometric head are given at intervals of 10 ft (solid lines, adapted from Chapelle and Drummond, 1983). Dotted lines represent a few exemplary estimated flow lines, manually drawn on the basis of the requirement to intersect head contours perpendicularly. Note that the direction of groundwater flow (arrows) is mainly towards the east and does not coincide with the southeasterly direction of dip and the alignment of the wells. The dashed line A-B indicates the location of the cross-section shown in Figure 2.

The stratigraphy of the region (Fig. 2) consists of a sequence of sandy layers acting as aquifers and silty to clayey layers acting as aquitards (Hansen, 1974). In most of the study region, the Magothy aquifer (Cretaceous) underlies the Aquia, separated by the confining beds of the Monmouth, Matawan (both Cretaceous), and Brightseat (Paleocene) formations. The Aquia aquifer is confined by the Marlboro clay (Paleocene/Eocene), a distinct layer of pinkish clay, and the lower, silty and clayey part of the Nanjemoy formation (Eocene). The upper, sandy part of the Nanjemoy formation acts as an aquifer and is

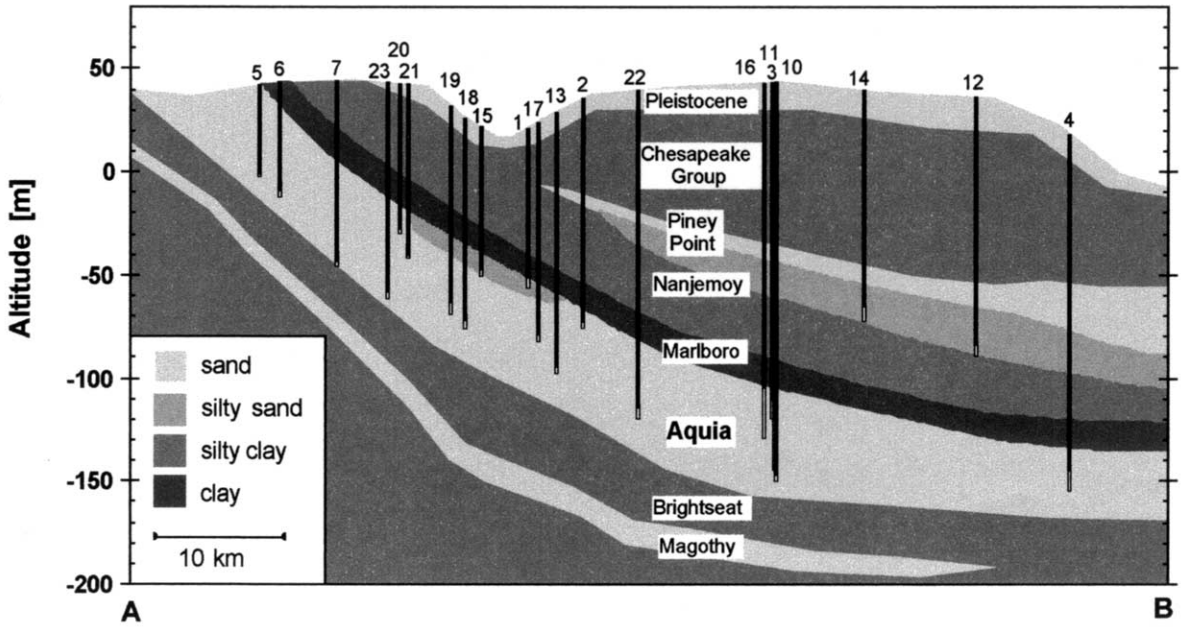

Fig. 2. Cross-section along line A-B indicated in Figure 1. The wells (solid black: casings, open: screens) are projected on this line, which does not coincide with a groundwater flowline. All wells except MD12 and 14 tap the Aquia formation, which forms the major aquifer in the region. Sand and silty sand layers act as aquifers, clay and silty clay layers as aquitards.

hydraulically connected to the overlying Piney Point aquifer (Eocene). The Aquia formation consists predominantly of quartz sand (50 to 75%), with a considerable amount of glauconite (20 to 40%), which gives the layer its characteristic greenish color. The abundance of carbonate shell debris is usually between 1 and 5%, but can reach up to 20% (Chapelle and Drummond, 1983). In some regions, intervals of drill cuttings were found to contain more than 25% of calcareously cemented sand and shell fragments (Hansen, 1974).

On the basis of the water chemistry, Chapelle and Drummond (1983) divided the Aquia aquifer into three approximately 40 km wide regions. The geochemical evolution proceeds from a calcium-magnesium-bicarbonate water in the outcrop area (region I) to a sodium-bicarbonate water in region III. The wells used in the present study are located in regions I and II, except for well MD4 that falls into region III.

Age estimates for Aquia water were derived from chloride concentrations (Purdy, 1991), as well as from some stable isotope and ^{14}C measurements (Purdy et al., 1992). The systematic variation of chloride concentration with distance from the outcrop in the Aquia aquifer was interpreted as a result of changes in meteoric deposition due to sea-level fluctuations. According to this hypothesis, the Cl^- minimum observed ~40 km from the outcrop area corresponds to the last glacial sea-level lowstand (~18 radiocarbon kyr BP), when the distance from the recharge area to the sea was nearly 200 km larger than at present. ^{14}C data from a site at a distance of 45 km from the outcrop indicated somewhat smaller ages (12 kyr from DIC and 17 kyr from DOC) after corrections for low initial ^{14}C activity as well as addition of dead carbon within the aquifer had been applied (Purdy et al., 1992). Purdy et al. (1996) re-interpreted the records of chloride concentrations and $^{36}Cl/Cl$ ratios in terms of a two-regions flow model. According to this model, the upper part of the aquifer was flushed more rapidly during times of low sea level due to increased hydraulic head gradients, placing the Cl^- minimum at younger ages. For the lowermost part of the aquifer, however, this model predicts very slow flow and ages of 100 kyr or more.

3. METHODS

3.1. Sampling and Analysis

Samples from a total of 23 wells were collected during three field campaigns in 1995. In the upgradient part of the aquifer it was necessary to rely on small wells that supply private homes, whereas further downgradient in Calvert County, where the aquifer is more productive, nine public water supply wells could be sampled. Well depths range from 12 m in the outcrop area to ~190 m in the confined part. Screens are usually a few meters long near the bottom of the wells (Fig. 2). Before sampling, wells were pumped sufficiently to flush the boreholes several times.

Water temperature, electrical conductivity, and pH were repeatedly measured during sampling to ensure that conditions remained stable. In the field, alkalinity and dissolved oxygen were determined by titration (Gran and Winkler methods, respectively) and a colorimetric test for nitrate concentration (CHEMets® test kits) was conducted. Samples for the analysis of carbon isotopes (^{13}C and ^{14}C) were collected in 500 mL glass bottles and preserved by adding 0.2 mL of saturated $HgCl_2$ solution. Samples for stable isotope analysis were taken in 60 mL glass bottles. Samples for the mass spectrometric measurement of noble gases were sealed off in copper tubes of ~40 cm^3 volume (Weiss, 1968), according to the procedures described in Stute et al. (1995a).

During sampling for dissolved gases, conditions that could lead to contact with the atmosphere or partial degassing of the samples have to be avoided. Despite all efforts, this goal could not always be achieved in this study. A major concern were pressure tanks, which were present in most private wells and might contain a gas phase. Samples were taken before the pressure tanks if possible, but at seven wells (MD1, 2, 5, 7, 9, 18, 23) the exact arrangement of the piping could not be verified and sampling conditions were thus deemed questionable for noble gases. An additional concern was low pressure and/or intermittent

pumping at wells MD2, 9, and 23. However, the effective quality of noble gas samples is best judged on the basis of the measured concentrations, because effects such as degassing or strong air contamination are usually evident in the data.

For carbon isotope analysis, the DIC was converted to CO_2, which was then extracted using the procedure described by Clark et al. (1997). Both $^{13}C/^{12}C$ and $^{14}C/^{12}C$ ratios were measured at Lawrence Livermore National Laboratory by conventional and accelerator mass spectrometry, respectively. ^{13}C results are reported as δ values relative to the PDB standard, and have an overall precision of $\pm 0.3‰$. ^{14}C results are normalized to the NBS OX-1 standard, corrected for background and isotopic fractionation using the measured $\delta^{13}C$ values, and reported as percent modern carbon (pmc). The analytical precision of the AMS ^{14}C results is $\pm 0.7\%$ and the background corresponds to a conventional ^{14}C age of 45 kyr or ~ 0.4 pmc (Roberts et al., 1997). In view of the uncertainties related to sample preparation we adopt an overall uncertainty of $\pm 1\%$ of the given value or at least ± 0.4 pmc.

Stable isotope ratios $\delta^{18}O$ and δD were measured at Mountain Mass Spectrometer. Duplicates of all samples were analyzed. Analytical uncertainties of the individual measurements are better than $\pm 0.1‰$ for $\delta^{18}O$ and $\pm 1‰$ for δD. Chemical analyses were performed at the University of Maryland. Major cations (Ca, Mg, Na, K) were analyzed by flame atomic absorption spectroscopy, anions (Cl, F, SO_4, NO_3) by ion chromatography.

The dissolved gases were extracted from the copper tubes on a vacuum line. The individual noble gases were separated and successively analyzed in a MAP 215-50 noble gas mass spectrometer. Details of the analytical procedure have been described by Stute et al. (1995a). Calibration curves accounting for the pressure dependence of the sensitivity were obtained by fitting simple polynomials to the results of repeated measurements of air aliquots of different size, covering the range found in the samples. The standard deviations of the air calibrations from the fit curves varied between ± 0.5 and 0.7% for Ne, Ar, Kr, and Xe. For He, the dynamic range was much larger and the scatter was $\pm 1.2\%$. Overall uncertainties of measured concentrations, including the reproducibility of sampling and gas extraction were estimated from analyses of 9 pairs of duplicate and one set of triplicate samples. The data from these individual measurements were combined by normalizing them to the respective mean values. Standard deviations of the normalized duplicate measurements were $\pm 1.4\%$ for He, $\pm 0.8\%$ for Ne (excluding one outlier), $\pm 0.7\%$ for Ar, $\pm 0.9\%$ for Kr, and $\pm 0.8\%$ for Xe. As expected, these errors are slightly larger than the reproducibility of the air standards.

For a few samples, tritium concentrations were determined by the ^{3}He-ingrowth method (Clarke et al., 1976). Between 200 and 500 mL of water sampled in glass bottles were degassed and flame-sealed in glass bulbs with low He permeability. After several weeks of storage, the ^{3}He which had accumulated from tritium decay was extracted and admitted to a VG-5400 He isotope mass spectrometer (Ludin et al., 1997). The analytical precision as well as the detection limit of the tritium measurements was approximately ± 0.1 TU (tritium units, 1 TU is equivalent to a $^3H/^1H$ ratio of 10^{-18}).

3.2. Interpretation of Noble Gas Data

The correct treatment of the "excess air" component (Heaton and Vogel, 1981) constitutes the principal difficulty in the interpretation of noble gases in groundwater. Three models of the formation of excess air have been proposed: total dissolution (TD) of trapped air bubbles, resulting in atmospheric composition of the excess air (e.g., Andrews and Lee, 1979; Stute and Schlosser, 1993); total dissolution followed by partial re-equilibration (PR) with the atmosphere, resulting in diffusivity-controlled fractionation of the excess air (Stute et al., 1995b); and closed-system equilibration (CE) of groundwater with only partially dissolved entrapped air, resulting in solubility-controlled fractionation (Aeschbach-Hertig et al., 2000).

As will be shown below, the CE-model provides the best description of the noble gas data set from the Aquia aquifer. The model equations are (Aeschbach-Hertig et al., 2000):

$$C_i(T,S,P,A,F) = C_i^*(T,S,P) + \frac{(1-F)Az_i}{1+FAz_i/C_i^*} \qquad (\text{i} = \text{He, Ne, Ar, Kr, Xe}) \quad (1)$$

where $C_i^*(T,S,P)$ are the moist air solubility equilibrium concentrations as functions of temperature, salinity, and atmospheric pressure (Clever, 1979; Weiss, 1970, 1971; Weiss and Kyser, 1978), and z_i are the noble gas volume fractions in dry air. A describes the initial amount of dry entrapped air per unit mass of water and F parameterizes the fractionation of excess air.

For the Aquia aquifer, as usual in noble gas studies of groundwater, Eqn. 1 is not applicable to the observed He because of the presence of radiogenic He, and the parameters P and S can be estimated. We used $P = 0.994$ atm corresponding to recharge at an altitude of 50 m, and $S = 0‰$ for the meteoric recharge water. Thus, Eqn. 1 describes four measured concentrations (Ne, Ar, Kr, Xe) with three free parameters (T, A, F). It was solved for the unknown parameters by inverse modeling as described by Aeschbach-Hertig et al. (1999). This nonlinear least squares method finds those values of the model parameters that minimize χ^2, the sum of the squared deviations between the modeled and measured concentrations, normalized to the respective experimental uncertainties. A χ^2-test can be used to judge the ability of different models to describe the data within their uncertainty, on the level of individual samples as well as the entire data set (Ballentine and Hall, 1999; Aeschbach-Hertig et al., 1999). We first applied the χ^2-test to individual samples to identify irregular samples that cannot be described by any model. In a second step we applied it to the entire set of "good" samples to select the appropriate excess air model. In both cases, we rejected samples or models that yield probabilities $p < 0.01$ (p is the probability to obtain a χ^2-value equal or higher than the observed value with a correct model).

The uncertainties of the estimated model parameters are calculated from the covariance matrix in the least squares fitting algorithm (Press et al., 1986). Numerical error propagation by Monte Carlo simulations usually confirms this error estimate (Aeschbach-Hertig et al., 1999). For samples with high χ^2-values, more conservative estimates of the uncertainties of the parameters may be derived by scaling the covariance matrix errors with the factor $(\chi^2/\nu)^{1/2}$, where ν is the number of degrees of freedom (Rosenfeld et al., 1967). This scaling implicitly estimates the uncertainty of the data from their deviation from the model. Because we have derived reliable experimental errors (see section 3.1.), this scaling does not seem indicated in general. Yet, for those samples that were rejected on the basis of the χ^2-test, the scaled errors may provide a tentative estimate of the reliability of the results.

The parameters derived from the inverse modeling of the heavier noble gases were used to calculate the atmospheric He component, and hence the radiogenic He excess (He_{rad}) as the difference between the measured total He and the calculated atmospheric He. This is the strictest way to derive He_{rad}, which is used for groundwater dating.

4. RESULTS

To detect general patterns in the distributions of the chemical and isotopic tracers, the results are plotted as a function of the distance from the outcrop region along hypothetical flow lines (Figs. 3 to 5). Flow lines and distances were roughly estimated on the basis of the prepumping potentiometric surface (Fig. 1, Chapelle and Drummond, 1983). The inferred flow lines start at the northern boundary of the outcrop area and bend from a southeasterly to an easterly direction (perpendicular to head contours, Fig. 1). Note that the sampled wells lie on several different flow lines and that flow lines may have been different in the past. The procedure to estimate flow distances is analogous to that used by Purdy (1991) and Purdy et al. (1992, 1996). Thus, our results can be compared to those of the earlier studies, although different wells were sampled (except MD1 and 2, which are wells no. 17 and 16 of Purdy et al., 1996).

On the basis of well logs and hydrogeologic information (Fig. 2), we conclude that two wells (MD12 and 14) draw water from the overlying Piney Point/Nanjemoy formation rather than the Aquia. Since the recharge area of the Piney Point

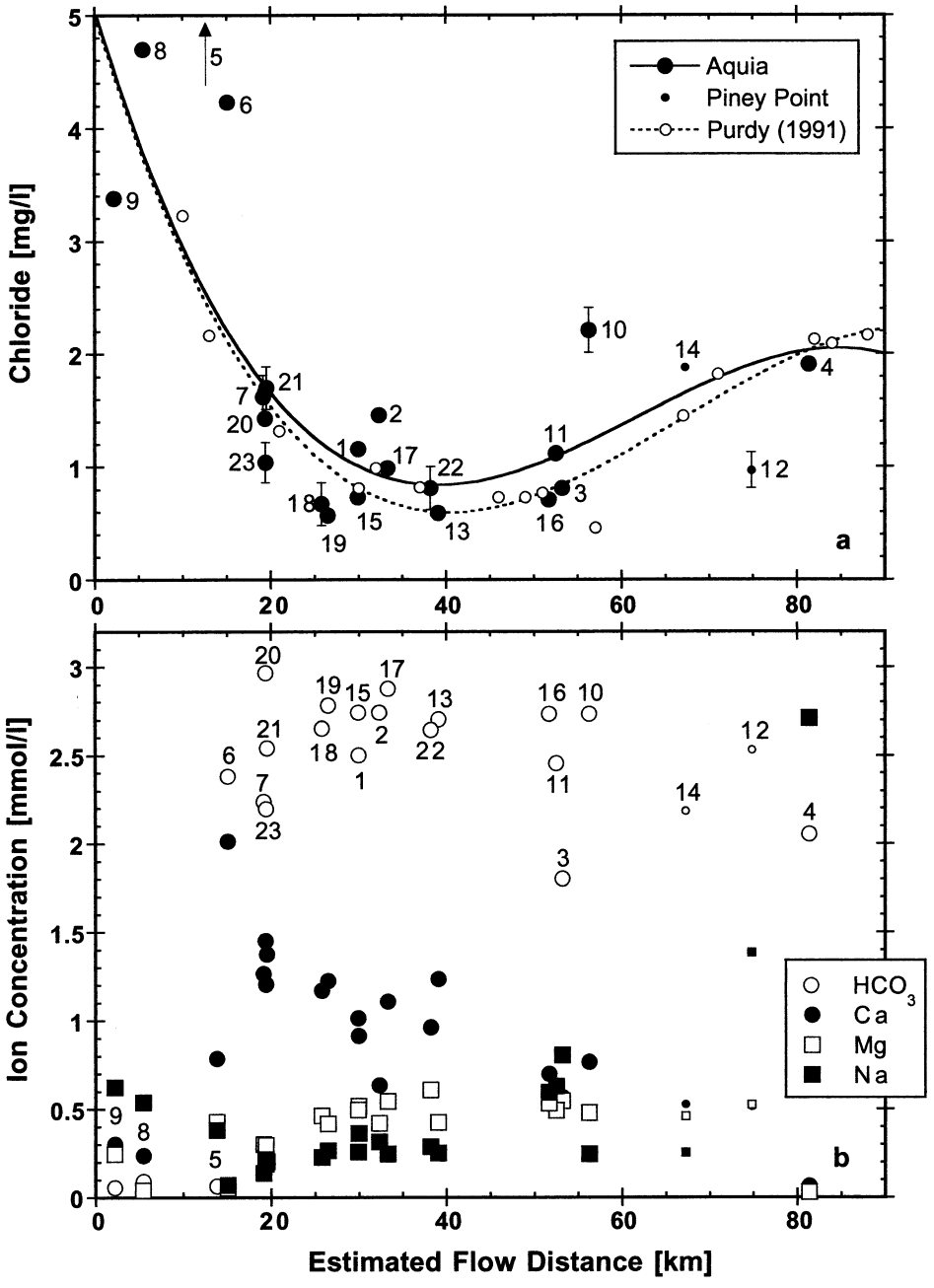

Fig. 3. Variation of ion concentrations with flow distance. Note that this and the following figures do not represent an evolution along one flowline. Large symbols represent samples from the Aquia aquifer, small symbols samples from the Piney Point formation (shown for comparison only on the Aquia aquifer distance scale). a) Chloride. Full symbols represent data of this study, open symbols samples from Purdy (1991), shown for reference. The dashed line is the third order polynomial fit applied by Purdy (1991) to their data, the solid line is the same fit through our Aquia data (except well MD5). The two data sets are in good agreement, both showing a chloride minimum at flow distances of ~40 km. b) Major ions. In the recharge area, concentrations rise rapidly due to calcite dissolution. Downstream of the outcrop, Ca^{2+} decreases slowly due to ion exchange and is replaced first by Mg^{2+} and later by Na^{+}, whereas HCO_3^- remains practically constant.

aquifer is not well defined, we do not establish a separate flow distance scale for this aquifer. The data from the Piney Point wells are plotted with small symbols on the Aquia distance scale in Figures 3–5, although a direct comparison on this scale may be misleading.

4.1. Chemistry

Purdy (1991) found a minimum in chloride concentrations at ~40 km flow distance, and interpreted it as reflecting the last glacial sea-level lowstand. The chloride data obtained in our

Table 1. Well data, field measurements, and results of chemical analyses.

Well	State permit no.	Distance [km]	Depth [m]	Temp [°C]	κ_{25} [μS/cm]	pH	Alk [meq/l]	Tot CO_2 [mmol/l]	Ca^{2+} [μg/g]	Mg^{2+} [μg/g]	Na^+ [μg/g]	K^+ [μg/g]	Cl^- [μg/g]	SO_4^{2-} [μg/g]	NO_3^- [μg/g]
MD9	AA-73-7132	2.2	15.2	16.0	178	4.7	0.06[a]	2.73	12.1	5.95	14.4	6.6	3.38	2.6	9.88
MD8	AA-92-0759	5.4	21.3	16.2	59	5.7	0.09[a]	0.59	9.5	0.95	12.4	2.8	4.70	0.3	1.89
MD5	AA-88-794	13.8	12.2	14.4	276	4.7	0.07[a]	3.28	31.5	10.34	8.7	8.3	24.57	73.9	2.85
MD6	AA-92-1790	15.1	21.3	15.0	255	6.9	2.38	3.10	80.7	1.29	1.6	4.0	4.23	4.5	0.79
MD7	AA-88-9608	19.1	95.1	15.2	276	7.0	2.24	2.78	50.7	7.26	3.2	5.0	1.62	33.3	<0.05[b]
MD20	PG-73-0702	19.3	84.1	14.7	279	7.7	2.98	3.12	58.2	5.39	5.0	5.9	1.43	4.6	0.014
MD23	PG-81-0691	19.4	111.2	15.3	250	7.7	2.21	2.30	48.4	7.12	4.3	5.0	1.04	9.7	0.296
MD21	PG-81-1568	19.5	91.4	14.5	267	7.6	2.55	2.70	55.2	4.96	4.7	5.0	1.70	8.0	0.021
MD18	PG-81-1187	25.8	96.0	14.6	280	7.8	2.67	2.77	47.0	11.23	5.2	10.1	0.67	9.1	0.030
MD19	CA-92-0082	26.5	83.8	14.1	276	7.7	2.79	2.93	49.1	10.09	6.1	8.5	0.57	6.4	0.021
MD15	CA-73-0196	29.9	102.1	15.4	280	7.8	2.76	2.85	40.7	11.98	5.9	11.7	0.73	8.3	0.053
MD1	PG-73-0506	30.0	109.4	15.6	254	7.7	2.51	2.64	36.6	12.51	8.3	17.0	1.16	5.8	0.026
MD2	CH-73-1818	32.3	134.1	14.5	269	7.7	2.76[a]	2.89	25.5	10.15	7.2	15.5	1.46	3.0	0.016
MD17	CA-92-0220	33.3	111.2	15.0	292	7.7	2.89	3.04	44.4	13.21	5.7	12.1	0.99	10.5	0.025
MD22	PG-92-0624	38.2	170.4	16.3	282	7.7	2.66	2.77	38.5	14.76	6.6	14.2	0.81	9.2	0.096
MD13	CA-88-0715	39.0	137.2	17.7	271	7.8	2.72	2.82	49.6	10.31	5.8	9.2	0.59	11.8	<0.05[b]
MD16	CA-72-0022	51.6	136.5	16.9	270	7.9	2.76	2.83	28.0	12.94	13.7	17.3	0.71	7.1	0.017
MD11	CA-73-2670	52.5	165.2	17.4	263	8.0	2.48	2.52	23.1	11.93	14.5	19.3	1.12	9.8	<0.05[b]
MD3	CA-88-2253	53.2	184.4	17.3	275	7.7	1.81	1.88	22.8	13.25	18.5	26.4	0.81	7.5	0.058
MD10	CA-88-0852	56.3	161.5	15.2	286	7.8	2.75[a]	2.85	30.8	11.62	5.6	13.8	2.21	12.0	<0.05[b]
MD14	CA-81-4117	67.3	91.4	14.9	242	7.8	2.20	2.27	21.2	11.16	5.8	16.3	1.88	10.3	0.028
MD12	CA-02-3170	74.8	122.5	16.8	265	8.1	2.57	2.59	20.7	12.76	31.9	21.7	0.97	18.9	<0.05[b]
MD4	CA-81-1193	81.3	189.0	17.9	223	8.8	2.17[a]	2.12	2.6	0.72	62.3	7.8	1.91	4.8	0.030
Error[c]				±0.2	±5	±0.1	±0.1	±0.1	±1.5	±0.15	±0.4	±0.2	±0.1	±0.2	±0.01

[a] Alkalinity calculated from measured pH and Total CO_2. Otherwise: Total CO_2 calculated from measured pH and alkalinity.
[b] Data from simple testkit only.
[c] Stated errors represent estimates of the typical uncertainty only.

study (Table 1) confirm this pattern, although they show a somewhat larger scatter (Fig. 3a). Empirical polynomial fits through the two data sets are very similar. The wells from the recharge area, in particular well MD5, have much higher chloride concentrations than the wells in the confined part of the aquifer. These elevated concentrations may be due to anthropogenic influence, as indicated also by high nitrate concentrations and the presence of bomb-produced ^3H and ^{14}C (see below).

The concentrations of the major ions change systematically with flow distance (Fig. 3b, Table 1). Three of the four wells from the outcrop area (MD5, 8 and 9) yield very acidic water (typical pH: 4.7), probably due to dissolved soil-gas CO_2. Unstable pH values due to degassing prevented the determination of the alkalinity by titration in the field. Approximate HCO_3^- concentrations were calculated from the total CO_2 measured later in the laboratory and the pH measured in the field. The Ca^{2+} concentrations are rather low in these acidic wells, but reach a maximum in the last outcrop well (MD6), where pH is neutral. The water of MD6 is dominated by Ca^{2+} and HCO_3^- ions, whereas further downstream Ca^{2+} is replaced by Mg^{2+} and Na^+. The most distant well (MD4) is dominated by Na^+ and HCO_3^- ions. This evolution of the Aquia water is in agreement with the patterns described by Chapelle and Drummond (1983) and Chapelle and Knobel (1985).

4.2. Stable Isotopes and ^{14}C

The stable isotope values $\delta^{18}O$ and δD scatter within the first 35 km of flow distance, but between 35 and 55 km they are consistently lower (Fig. 4a, Table 2). A similar difference exists between the two wells from the Piney Point formation. The deuterium excess $d = \delta D - 8 \cdot \delta^{18}O$ (Table 2) varies quite strongly without an apparent relation to the stable isotope ratios or the flow distance. The scaling of Figure 4a is such that for samples that fall on the global meteoric water line (GMWL, defined by $\delta D = 8 \cdot \delta^{18}O + 10$) the points representing δD and $\delta^{18}O$ values would fall together. This is the case for two samples only (MD4 and 21). For most samples, the δD points lie somewhat beneath the $\delta^{18}O$ points, corresponding to deuterium excesses between 6 and 9.

The wells in the outcrop area have ^{14}C activities in DIC close to the modern (prebomb) level (Fig. 4b, Table 2). Bomb-produced ^{14}C is present at least in well MD9 (122 pmc). In the confined part of the aquifer, ^{14}C values generally decrease exponentially with flow distance (Fig. 4b) as would be expected if flow distance were a good proxy for flow time and the decrease of ^{14}C activities were only due to radioactive decay. However, there are important deviations from this trend, especially around flow distances of ~30 km, where several samples have activities below the detection limit of 0.4 pmc. Note that the apparent increase of ^{14}C activities at larger flow distances does not reflect a real evolution of the groundwater, because the wells are located on different flow lines.

$\delta^{13}C$ initially increases from values between −20 and −15‰ in the recharge area to an approximately constant value of −11‰ up to a flow distance of 60 km. In the most distant Aquia well (MD4), $\delta^{13}C$ rises to a value of −8‰. These observations are in agreement with published data (Chapelle and Knobel, 1985).

^{14}C dating of groundwater involves the calculation of the

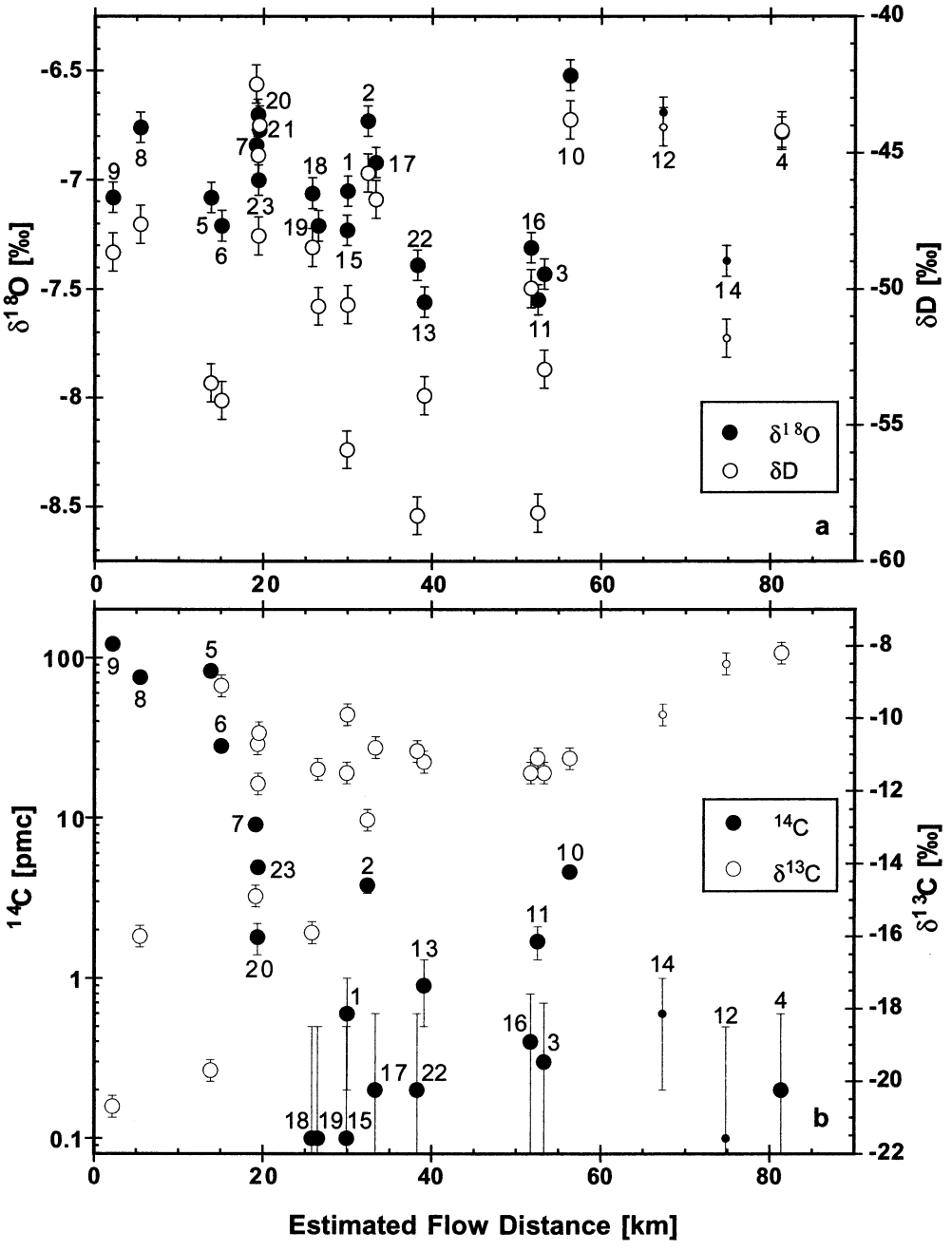

Fig. 4. Variation of isotope data with flow distance. Large symbols represent samples from the Aquia aquifer, small symbols samples from the Piney Point formation. a) Stable isotopes. Both $\delta^{18}O$ and δD are lowest between flow distances of 35 and 55 km. The vertical scales are such that points that lie on the global meteoric water line ($\delta D = 8 \cdot \delta^{18}O + 10$) fall together. Most wells have a deuterium excess below 10, thus δD-values plot below $\delta^{18}O$-values. b) Carbon isotopes. ^{14}C decreases roughly exponentially (note the logarithmic scale) with distance, except for a group of wells with very low activities between 25 and 40 km. $\delta^{13}C$ increases in the outcrop area to rather uniform values around −11‰.

initial ^{14}C activity of the DIC resulting from a mixture of soil CO_2 with variable ^{14}C values and solid carbonate that has ^{14}C values close to zero. Using measured variables such as alkalinity, total dissolved carbon, and $\delta^{13}C$, several models have been developed for estimating initial ^{14}C values. As a first approximation, we calculated ^{14}C ages according to the model introduced by Fontes and Garnier (1979), using typical values for the isotopic compositions of soil CO_2 and calcite (Table 2). By comparison, using the model of Ingerson and Pearson (1964), we obtain ages that are on average 4% higher, whereas the model of Tamers (1975) yields typically 10% higher ages. The ages are modern for the four wells from the outcrop area, but then jump to 15 kyr and rapidly increase to values of more than 30 kyr.

Table 2. Isotope data.

Well	Distance [km]	$\delta^{18}O$ [‰]	δD [‰]	d[a] [‰]	$\delta^{13}C$ [‰]	^{14}C [pmc]	^{14}C age[b] [kyr]
MD9	2.2	−7.08	−48.65	7.95	−20.7	121.7	modern
MD8	5.4	−6.76	−47.63	6.46	−16.0	75.5	modern
MD5	3.8	−7.08	−53.45	3.20	−19.7	83.1	modern
MD6	15.1	−7.21	−54.09	3.59	−9.1	28.2	modern
MD7	19.1	−6.84	−42.48	12.25	−14.9	9.1	15.5
MD20	19.3	−6.70	−45.09	8.47	−10.7	1.8	24.4
MD23	19.4	−7.00	−48.05	7.96	−11.8	4.9	18.1
MD21	19.5	−6.77	−43.99	10.14	−10.4	-[c]	-[c]
MD18	25.8	−7.06	−48.47	7.97	−15.9	0.1	>42
MD19	26.5	−7.21	−50.63	7.06	−11.4	0.1	>37
MD15	29.9	−7.23	−55.90	1.94	−11.5	0.1	>37
MD1	30.0	−7.05	−50.57	5.79	−9.9	0.6	31.6
MD2	32.3	−6.73	−45.74	8.06	−12.8	3.8	21.4
MD17	33.3	−6.92	−46.71	8.61	−10.8	0.2	>33
MD22	38.2	−7.39	−58.32	0.80	−10.9	0.2	>34
MD13	39.0	−7.56	−53.91	6.53	−11.2	0.9	31.1
MD16	51.6	−7.31	−49.98	8.46	−11.5	0.4	>33
MD11	52.5	−7.55	−58.22	2.19	−11.1	1.7	26.2
MD3	53.2	−7.43	−52.94	6.50	−11.5	0.3	>34
MD10	56.3	−6.52	−43.79	8.33	−11.1	4.6	17.5
MD14	67.3	−6.69	−44.05	9.47	−9.9	0.6	32.3
MD12	74.8	−7.37	−51.80	7.12	−8.5	0.1	>31
MD4	81.3	−6.78	−44.19	10.05	−8.2	0.2	>29
Errors		±0.07	±0.7		±0.3	±0.4[d]	

[a] Deuterium excess $d = \delta D - 8\delta^{18}O$.
[b] ^{14}C age calculated according to Fontes and Garnier (1979), assuming $\delta^{13}C$ values of −25 and 0‰, and ^{14}C activities of 100 and 0 pmc for soil CO_2 and calcite, respectively. For measured activities $A \leq 0.4$ pmc, minimum ages corresponding to $(A + 0.4)$ pmc are given.
[c] Sample lost.
[d] Or ±1% of the value for activities above 40 pmc.

4.3. Noble Gases

The different conceptual models for the excess air component in groundwater discussed by Aeschbach-Hertig et al. (2000) were fitted to the noble gas concentrations from all 29 samples (Table 3) using the inverse algorithm of Aeschbach-Hertig et al. (1999). The ability of the models to explain the data was checked by a χ^2-test (see section 3.2.). Five samples from three wells (MD1, 7, 23) could not be described by any available model ($p \ll 0.01$). All three wells belong to the group of wells where bypassing of the pressure tank could not be verified (see section 3.1.). Therefore, it seems likely that these samples were affected by artefacts induced during sampling, such as gas exchange in the pressure tank. All other samples, including those from the remaining wells with questionable sampling conditions (MD 2, 5, 9, 18), yield acceptable fits, at least with the CE-model (Eqn. 1). Thus, the inverse evaluation procedure seems to enable an objective judgment of sample quality.

After elimination of the problematic samples (MD1, 7, 23), the χ^2-test was applied to the remaining data set to choose the appropriate excess air model. Even with slightly larger error estimates (±1% on all concentrations) as used in Aeschbach-Hertig et al. (2000), this test showed that only the CE-model is applicable. With the more stringent error estimates used here, the CE-model is still acceptable (29 samples, $\chi^2 = 49$, $p = 0.011$). Other models clearly fail ($\chi^2 > 100$, $p < 10^{-8}$ for both TD and PR-model). The results obtained with the CE-model are summarized in Table 4.

Temperature results from replicate samples usually agree within 0.2°C, except for well MD2 where they differ by ~0.6°C and MD4 where one of three samples differs by more than 1°C from the other two. Mean concentrations for wells with replicate samples were calculated and evaluated by the inverse technique. The parameters derived from fitting these mean concentrations are almost identical to the weighted means of the parameters derived from the individual samples. The same holds true for the correctly propagated errors of the mean values. This result confirms the robustness of the inverse technique to derive NGTs and their uncertainties.

Weighted mean NGTs (Table 5) are used in the following discussion. An exception is made for well MD18, where both samples individually yield acceptable fits ($p \approx 0.03$), but the fit of the mean concentrations with accordingly reduced errors is below our cutoff criterion ($p = 0.002$). In this case, we use the weighted mean results with uncertainties as derived from the individual samples. The best results of the rejected fits from wells MD1, 7, and 23 are also listed in Table 5 and shown in subsequent figures, using the scaling of the errors by the factor $(\chi^2/\nu)^{1/2}$. Yet, as these results are based on insufficient modeling of the data, we do not include them in the further discussion.

The model parameters A and F have a physical interpretation that should be used to check the plausibility of the fit results (Aeschbach-Hertig et al., 2000, 2001). A describes the initial volume of entrapped air per unit volume of water. F can be expressed as the ratio of two parameters with a physical mean-

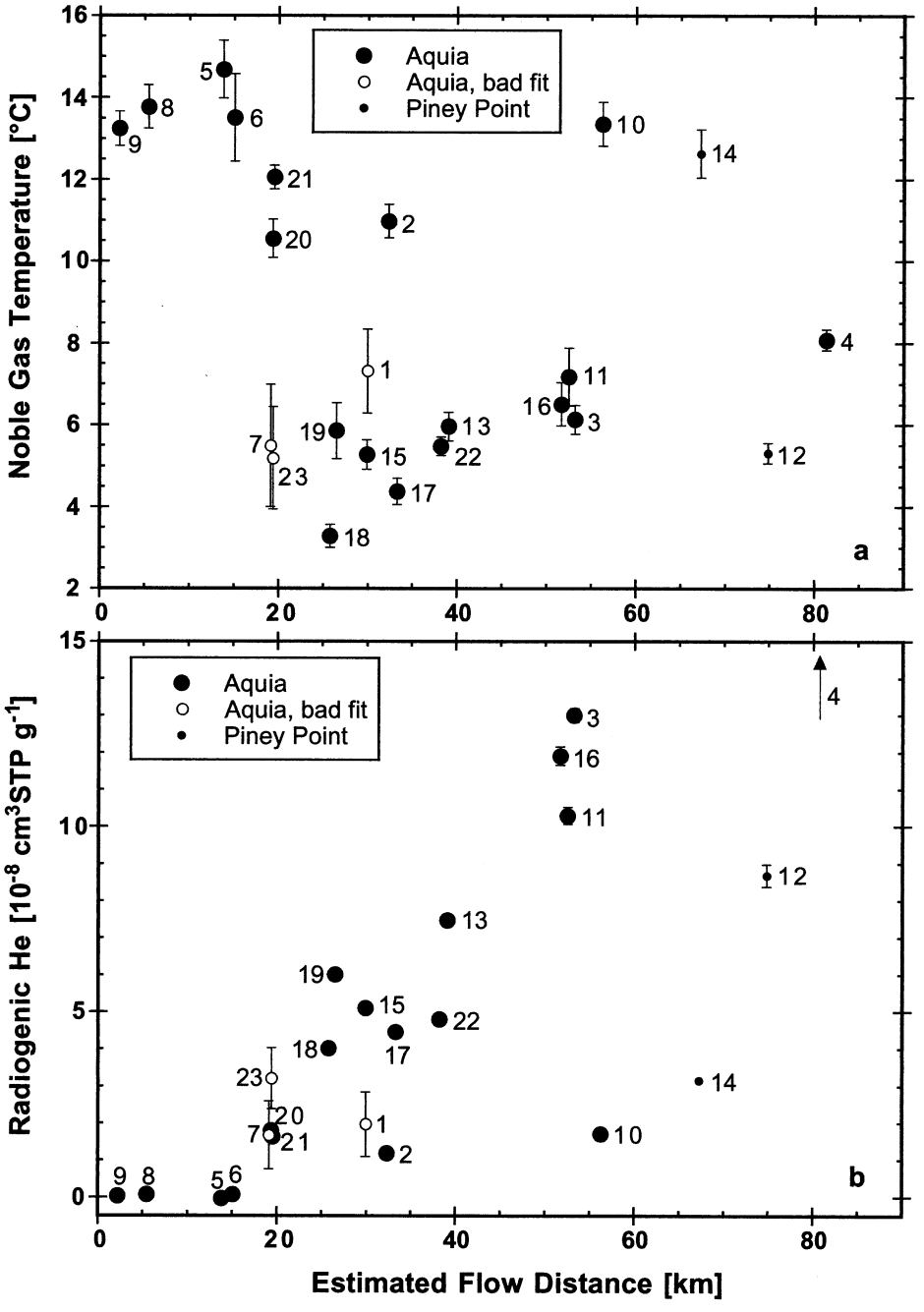

Fig. 5. Variation of noble gas results with flow distance. Large solid symbols represent regular samples from the Aquia aquifer, small solid symbols samples from the Piney Point formation. Open symbols indicate best estimates for samples that could not be described by any model for noble gases in groundwater, probably due to inadequate sampling conditions. These tentative results are not considered in the discussion. a) Noble gas temperature (NGT). NGT drops sharply between 20 and 25 km, and then rises gradually (except for the high value at MD10). b) Radiogenic He. The approximately linear increase of He concentrations with flow distance is broken only by the low value at MD10, the high value at MD4 (off scale) and the displacement of the Piney Point wells (MD12 and 14).

ing: $F = v/q$, where v is the ratio of the entrapped gas volumes in the final and initial state, and q is the ratio of the dry gas pressure in the trapped gas to that in the free atmosphere. Thus, F describes the reduction of the trapped air volume A by partial dissolution (v) and compression ($1/q$). The resulting excess of dissolved gases, which is often expressed by the relative Ne excess ΔNe, is related to the dissolved fraction ($1-v$) of the entrapped air (A) and the pressure (q) acting on the entrapped gas (Aeschbach-Hertig et al., 2001).

On the basis of field data of Fayer and Hillel (1986) on the

Table 3. Noble gas data.

Sample	He [10^{-8} cm^3 STP g^{-1}]	Ne [10^{-7} cm^3 STP g^{-1}]	Ar [10^{-4} cm^3 STP g^{-1}]	Kr [10^{-8} cm^3 STP g^{-1}]	Xe [10^{-8} cm^3 STP g^{-1}]	^{3}He/^{4}He 10^{-6}
MD9.1	5.988	2.493	4.020	8.985	1.221	2.59
MD8.2	5.529	2.303	3.894	8.757	1.198	2.83
MD5.2	5.413	2.295	3.883	8.638	1.179	1.67
MD6.2	5.107	2.145	3.835	8.756	1.215	4.69
MD7.1	8.070	2.714	4.533	10.14	1.634	1.11
MD7.2	8.140	2.716	4.548	10.28	1.639	1.13
MD20.2	7.220	2.324	4.153	9.302	1.334	1.09
MD23.1	9.213	2.554	4.537	10.38	1.617	0.899
MD21.1	7.059	2.306	3.976	8.891	1.259	1.10
MD21.2	7.095	2.308	3.968	8.863	1.258	1.10
MD18.1	9.785	2.560	4.846	11.30	1.724	0.849
MD18.2	9.945	2.559	4.832	11.23	1.714	0.855
MD19.1	11.87	2.584	4.906	11.36	1.626	0.726
MD15.2	10.89	2.530	4.728	10.84	1.610	0.787
MD1.1	14.47	4.817	5.517	11.09	1.613	1.17
MD1.3	13.79	4.529	5.383	10.97	1.583	1.18
MD2.1	7.265	2.557	4.428	9.718	1.368	1.18
MD2.2	7.022	2.522	4.338	9.699	1.337	1.19
MD17.2	10.02	2.444	4.703	10.90	1.650	0.818
MD22.1	10.53	2.467	4.611	10.71	1.587	0.835
MD22.2	10.28	2.422	4.552	10.50	1.576	0.783
MD13.1	13.18	2.575	4.782	11.03	1.589	0.655
MD13.2	13.44	2.543	4.784	11.18	1.597	0.638
MD16.1	17.51	2.480	4.663	10.80	1.555	0.491
MD11.1	15.92	2.456	4.622	10.75	1.531	0.508
MD3.3	18.66	2.475	4.637	11.02	1.560	0.450
MD3.4	18.69	2.488	4.673	10.99	1.571	0.438
MD10.1	7.491	2.437	4.070	8.959	1.234	1.07
MD14.1	8.830	2.407	4.128	9.095	1.267	0.936
MD12.1	26.00	6.733	7.148	14.08	1.833	0.933
MD12.2	26.62	6.992	7.294	14.22	1.841	0.919
MD4.1	50.03	2.512	4.487	10.16	1.432	0.160
MD4.3	52.29	2.496	4.503	10.50	1.471	0.179
MD4.4	52.06	2.523	4.499	10.06	1.478	0.169
Errors	±1.4%	±0.8%	±0.7%	±0.9%	±0.8%	±5%

volume fraction of entrapped air, A is expected to range from 0.02 to 0.18 cm^{3}STP g^{-1}. Assuming seasonal water table fluctuations of up to 2 m, q should fall between 1 and 1.2. Such pressures could force at most ~0.004 cm^{3}STP g^{-1} of air into dissolution, or 2 to 20% of the expected entrapped air, suggesting that v should fall between 0.8 and 0.98. The results for the Aquia samples fall in or close to the expected range (A: 0.01 to 0.07 cm^{3}STP g^{-1}, v: 0.72 to 0.94, q: 1.10 to 1.23, Table 4). However, there are two noticeable exceptions.

Sample MD6 yields an unrealistically high value of A that, however, seems to be rather accidental, because its uncertainty is huge ($A = (0.29 \pm 0.89)$ cm^{3}STP g^{-1}). Obviously, A is not well constrained by the data. Prescribing A-values in the expected range (0.02 to 0.18 cm^{3}STP g^{-1}), we obtain good fits (χ^2 decreasing from 2.7 to 0.05) with temperatures increasing from 12.4 to 14.0°C. As our best estimate for T, we use the result obtained at $A = 0.1$ cm^{3}STP g^{-1}, with an error that includes the whole range ($T = 13.5 \pm 1.1$°C, Table 5). This result is supported by Monte Carlo simulations, for which 1000 input data sets were randomly drawn from the distributions defined by the measured data and their experimental uncertainties (see Aeschbach-Hertig et al., 1999). Fitting these data yielded a distribution of T-values with a mean of 13.6°C and a standard deviation of 0.8°C.

The second exceptional case is well MD12, where both samples yield very high values of q (≈2.3) and low values of v (0.20). These samples have by far the highest noble gas concentrations, due to a large excess air component (ΔNe ≈ 230%). This high excess does not appear to be due to air contamination during sampling, because the excess air is fractionated and the duplicate samples reproduced well. Yet, the interpretation of the large excess air component as a result of almost complete dissolution of the entrapped air due to high pressures is consistent with the data and yields reasonable results.

The NGTs vary systematically with flow distance (Fig. 5a, Table 5). They are highest (≈14°C) at distances less than 15 km, and drop to values between 3 and 6°C at distances around 30 km from the outcrop. At distances larger than ~50 km, the temperatures gradually rise up to 8°C. Only two Aquia samples (MD2 and 10) do not fit into this pattern. MD10 yields a temperature similar to the wells from the outcrop area although it lies at a flow distance of almost 60 km. The two wells from the Piney Point aquifer also show a large difference in NGT, although displaced to large distances when plotted on the Aquia scale.

4.4. He Isotopes and Tritium

Two different non-atmospheric He components can be identified on the basis of the He isotopes (Table 3): The

Table 4. Results of fitting equation 1 to the measured concentrations of Ne, Ar, Kr, and Xe.

Sample	χ^2	p	T [°C]	A [cm^{3}STP/g]	F	q	ν	ΔNe [%]	radiogenic He [10^{-8} cm^{3}STP/g]
MD9.1	1.29	0.26	13.2 ± 0.4	0.020	0.66	1.20	0.80	28.1	0.04 ± 0.10
MD8.2	0.56	0.46	13.8 ± 0.5	0.031	0.79	1.15	0.90	18.9	0.07 ± 0.09
MD5.2	0.05	0.83	14.7 ± 0.7	0.045	0.80	1.16	0.93	19.5	−0.03 ± 0.09
MD6.2	0.03	0.87	14.4 ± 2.6	0.288	0.89	1.11	0.99	11.4	0.05 ± 0.11
MD7.1	*66.1*	*0.00*	*5.5 ± 0.3*	*0.003*	*0.00*	*1.14*	*0.00*	*29.5*	*1.63 ± 0.17*
MD7.2	*51.0*	*0.00*	*5.3 ± 0.3*	*0.003*	*0.00*	*1.14*	*0.00*	*29.3*	*1.70 ± 0.17*
MD20.2	2.64	0.10	10.6 ± 0.5	0.030	0.81	1.13	0.91	16.5	1.80 ± 0.11
MD23.1	*21.0*	*0.00*	*5.1 ± 0.3*	*0.002*	*0.00*	*1.10*	*0.00*	*21.3*	*3.21 ± 0.18*
MD21.1	1.08	0.30	12.1 ± 0.4	0.020	0.77	1.13	0.87	17.3	1.62 ± 0.11
MD21.2	1.43	0.23	12.0 ± 0.4	0.018	0.76	1.12	0.86	17.4	1.65 ± 0.11
MD18.1	4.29	0.04	3.2 ± 0.3	0.010	0.65	1.11	0.72	18.9	3.94 ± 0.16
MD18.2	4.99	0.03	3.4 ± 0.3	0.010	0.65	1.11	0.72	19.1	4.10 ± 0.16
MD19.1	0.01	0.93	5.9 ± 0.7	0.072	0.78	1.20	0.93	23.6	6.01 ± 0.17
MD15.2	2.87	0.09	5.3 ± 0.4	0.024	0.75	1.14	0.86	20.3	5.11 ± 0.16
MD1.1	*27.9*	*0.00*	*7.1 ± 0.3*	*0.015*	*0.00*	*1.68*	*0.00*	*134*	*1.90 ± 0.27*
MD1.3	*17.4*	*0.00*	*7.3 ± 0.3*	*0.014*	*0.00*	*1.61*	*0.00*	*120*	*2.01 ± 0.26*
MD2.1	2.55	0.11	10.7 ± 0.6	0.042	0.72	1.23	0.88	28.4	1.28 ± 0.12
MD2.2	0.05	0.82	11.3 ± 0.6	0.046	0.73	1.22	0.90	27.4	1.12 ± 0.11
MD17.2	4.69	0.03	4.4 ± 0.3	0.017	0.78	1.10	0.86	15.1	4.47 ± 0.15
MD22.1	1.14	0.29	5.4 ± 0.3	0.017	0.75	1.12	0.84	17.4	4.89 ± 0.16
MD22.2	4.28	0.04	5.6 ± 0.3	0.014	0.75	1.10	0.83	15.5	4.74 ± 0.16
MD13.1	0.01	0.93	6.0 ± 0.5	0.042	0.76	1.18	0.90	23.3	7.31 ± 0.19
MD13.2	0.61	0.43	5.9 ± 0.5	0.055	0.78	1.18	0.92	21.8	7.66 ± 0.20
MD16.1	0.01	0.92	6.5 ± 0.5	0.049	0.80	1.16	0.92	19.4	11.86 ± 0.25
MD11.1	0.19	0.67	7.2 ± 0.7	0.068	0.81	1.16	0.94	19.1	10.32 ± 0.23
MD3.3	4.30	0.04	6.2 ± 0.5	0.046	0.80	1.15	0.92	18.8	13.04 ± 0.27
MD3.4	1.23	0.27	6.1 ± 0.5	0.045	0.80	1.15	0.92	19.3	13.03 ± 0.27
MD10.1	0.22	0.64	13.4 ± 0.5	0.033	0.73	1.20	0.88	25.4	1.71 ± 0.12
MD14.1	1.17	0.28	12.6 ± 0.6	0.040	0.76	1.19	0.90	23.0	3.15 ± 0.13
MD12.1	0.27	0.60	5.3 ± 0.4	0.036	0.09	2.23	0.20	220	8.73 ± 0.42
MD12.2	0.13	0.71	5.4 ± 0.4	0.038	0.09	2.30	0.20	233	8.64 ± 0.43
MD4.1	0.01	0.91	9.1 ± 0.5	0.045	0.76	1.19	0.90	24.2	44.22 ± 0.70
MD4.3	2.68	0.10	7.9 ± 0.5	0.038	0.77	1.17	0.90	21.9	46.56 ± 0.73
MD4.4	6.26	0.01	7.8 ± 0.4	0.021	0.71	1.16	0.83	23.1	46.21 ± 0.73

χ^2 is the sum of the weighted squared deviations between modeled and measured concentrations. Its expected value is the number of degrees of freedom, which is one, since there are four constraints (Ne, Ar, Kr, Xe) and three free parameters (T, A, F) for each sample.

p is the probability for χ^2 to be equal to or larger than the actual value due to random errors, although the model is correct. Fits with $p < 0.01$ are rejected (values in italics). The respective samples yield $F = 0$ (no fractionation) and cannot be described by any other available model.

T is the model parameter for the equilibration temperature (noble gas temperature, NGT).

A is the model parameter for the STP-volume of initially entrapped air per mass of water.

$F = \nu/q$ is the fractionation parameter, reflecting the reduction of the entrapped gas volume.

ν is the remaining fraction of the entrapped gas volume after partial dissolution.

q is the dry gas pressure in the entrapped gas relative to that in the atmosphere.

$\Delta Ne\ (\%) = (Ne_{meas}/Ne_{eq} - 1) \cdot 100\%$ is the relative Ne excess above solubility equilibrium.

Radiogenic He is the He excess above the atmospheric He components predicted by the model.

wells from the outcrop area (MD5, 6, 8, 9) have $^3He/^4He$ ratios above the atmospheric value ($1.384 \cdot 10^{-6}$, Clarke et al., 1976), indicating accumulation of ^3He from tritium decay, whereas all other wells have $^3He/^4He$ ratios below the atmospheric value, indicating accumulation of radiogenic He. These non-atmospheric He components are calculated from the measured He by subtracting the equilibrium and excess air components, as defined by Eqn. 1 with the parameters obtained from the fit to the other noble gases. The correct choice of the excess air model can be crucial for this calculation (Aeschbach-Hertig et al., 2000). For the wells from the outcrop area, the assumption of unfractionated excess air would result in negative radiogenic He, whereas the assumption of fractionation by partial diffusive re-equilibration (Stute et al., 1995b) would imply unrealistically large concentrations of radiogenic He. The CE-model (Eqn. 1) yields not only the best fit for the heavier noble gases but also the most realistic results for the radiogenic He, i.e., values close to zero for the outcrop wells (Tables 4 and 5).

The concentrations of radiogenic He increase quasi-linearly with flow distance in the Aquia aquifer (Fig. 5b). Wells MD12 and 14 indicate a similar increase in the Piney Point aquifer, but shifted to larger distances if plotted on the Aquia distance scale. Only two Aquia wells deviate substantially from the linear trend: MD10 which lies clearly below the trend, and MD4, which has more than twice as much radiogenic ^4He as predicted by the trend (out of scale in Fig. 5b). All five noble gases consistently characterize well MD10 as young and warm, presumably of Holocene age, despite its location far from the recharge area. This well may be influenced by leakage from

Table 5. Final NGTs, radiogenic He, and He age assigned to wells.

Well	Distance [km]	NGT[a] [°C]	He_{rad}[a] [10^{-8} cm^3STP g^{-1}]	He age[b] [kyr]
MD9	2.2	13.2 ± 0.4	0.04 ± 0.10	0.2 ± 0.6
MD8	5.4	13.8 ± 0.5	0.07 ± 0.09	0.4 ± 0.6
MD5	3.8	14.7 ± 0.7	−0.03 ± 0.09	−0.2 ± 0.5
MD6[c]	15.1	13.5 ± 1.1	0.07 ± 0.08	0.4 ± 0.5
MD7[d]	19.1	*5.5 ± 1.5*	*1.67 ± 0.92*	*10.1 ± 5.7*
MD20	19.3	10.6 ± 0.5	1.80 ± 0.11	10.9 ± 1.6
MD23[d]	19.4	*5.2 ± 1.3*	*3.21 ± 0.82*	*19.5 ± 5.6*
MD21	19.5	12.1 ± 0.3	1.63 ± 0.08	9.9 ± 1.4
MD18	25.8	3.3 ± 0.3	4.02 ± 0.16	24.4 ± 3.3
MD19	26.5	5.9 ± 0.7	6.01 ± 0.17	36.5 ± 4.8
MD15	29.9	5.3 ± 0.4	5.11 ± 0.16	31.1 ± 4.1
MD1[d]	30.0	*7.3 ± 1.0*	*1.97 ± 0.87*	*12.0 ± 5.5*
MD2	32.3	11.0 ± 0.4	1.19 ± 0.08	7.2 ± 1.1
MD17	33.3	4.4 ± 0.3	4.47 ± 0.15	27.1 ± 3.6
MD22	38.2	5.5 ± 0.2	4.81 ± 0.11	29.2 ± 3.8
MD13	39.0	6.0 ± 0.4	7.48 ± 0.14	45.5 ± 5.9
MD16	51.6	6.5 ± 0.5	11.9 ± 0.3	72.0 ± 9.4
MD11	52.5	7.2 ± 0.7	10.3 ± 0.2	62.7 ± 8.2
MD3	53.2	6.1 ± 0.3	13.0 ± 0.2	79 ± 10
MD10	56.3	13.4 ± 0.5	1.71 ± 0.12	10.4 ± 1.5
MD14	67.3	12.6 ± 0.6	3.15 ± 0.13	(19.2 ± 2.6)
MD12	74.8	5.3 ± 0.3	8.68 ± 0.30	(52.8 ± 7.0)
MD4	81.3	8.1 ± 0.3	45.6 ± 0.4	277 ± 36

[a] For wells with duplicate samples, weighted means were calculated.
[b] He age = He_{rad}/A_{He} with $A_{He} = (1.6 \pm 0.2) \cdot 10^{-12}$ cm^3STP g^{-1} yr^{-1} (Eq. 2). A_{He} is valid for the Aquia aquifer, thus ages for the Piney Point wells (MD12, 14) are tentative (values in parentheses).
[c] Results for well MD6 were estimated from fits with restricted range of the parameter A, best value taken for $A = 0.1$ cm^3STP g^{-1} (see text).
[d] For wells MD1, 7, and 23 (bad fits), the best fit results with scaled errors are given as tentative estimates (values in italics).

overlying aquifers or local mixing with young waters. Degassing during sampling appears unlikely, since the noble gas concentration pattern is consistent with Eqn. 1.

The high radiogenic He excess at well MD4 may be explained by the two-regions flow model of Purdy et al. (1996), which predicts very high ages in the lowermost part of the aquifer. Alternatively, one may assume a larger He accumulation rate due to a He flux from deeper strata. Such a flux may be particularly important at site MD4 either because of the large residence time, allowing the He to diffuse vertically through the aquifer (Torgersen and Ivey, 1985), or because of the absence of the underlying Magothy aquifer, which otherwise might capture the He flux.

Because of its high He concentration, well MD4 yields the best constraints for the isotopic signature of the radiogenic He in the Aquia aquifer and the contribution of ^{3}He from the decay of prebomb tritium in the groundwater. The non-atmospheric He component in this well, calculated on the basis of the fit of Eqn. 1 to the other noble gases, has a $^3He/^4He$ ratio of $(1.8 \pm 0.9) \cdot 10^{-8}$, typical for crustal radiogenic He (e.g., Mamyrin and Tolstikhin, 1984). This value is a maximum estimate, because part of the non-atmospheric ^{3}He may be tritiogenic. The non-atmospheric ^{3}He corresponds to a maximum prebomb tritium value of (3.3 ± 1.7) TU. The He data of all other wells are consistent with these upper limits for the radiogenic $^3He/^4He$ ratio and the prebomb tritium concentration.

Six samples (MD4, 5, 6, 7, 10, 14) were analyzed for tritium. Tritium concentrations in the two wells from the recharge area are substantial (13 TU at MD5 and 22 TU at MD6). By combining these results with the excess of tritiogenic ^{3}He, we can calculate $^3H/^3He$-ages (e.g., Schlosser et al., 1988) of 7 yr for MD5 and 25 yr for MD6. In contrast, tritium concentrations are very low (≤0.1 TU) in the wells from the confined part of the aquifer, indicating negligible addition of water younger than 50 yr to these wells, including well MD10 with its Holocene noble gas signature.

5. DISCUSSION

5.1. Climate Signals in Noble Gas and Stable Isotope Records

NGTs from the Aquia aquifer strongly suggest the presence of water from the last glacial period (LGP) at flow distances larger than ~25 km (Fig. 5a). This hypothesis is consistent with the interpretation of the chloride minimum (Fig. 3a) as due to the last glacial sea-level lowstand (Purdy, 1991). A plot of chloride concentration versus NGT (Fig. 6a) confirms the existence of a link between these quantities in our study area. With the exception of the samples from the outcrop area (MD5, 6, 8, 9), which exhibit anthropogenically enhanced chloride values, and the most distant well (MD4), all data, including those from the Piney Point aquifer, define a linear correlation between chloride and NGT ($r = 0.92$). This finding corroborates the interpretation of chloride as a climate indicator and of the observed NGT minimum at distances between 25 and 40 km as representative for the LGM.

A similar climate signal may be expected in the stable isotope ratios. At first sight, the plot of $\delta^{18}0$ versus NGT (Fig. 6b) does not show a systematic relationship. Yet, two major data clusters may be identified, a "cold" cluster with low $\delta^{18}0$

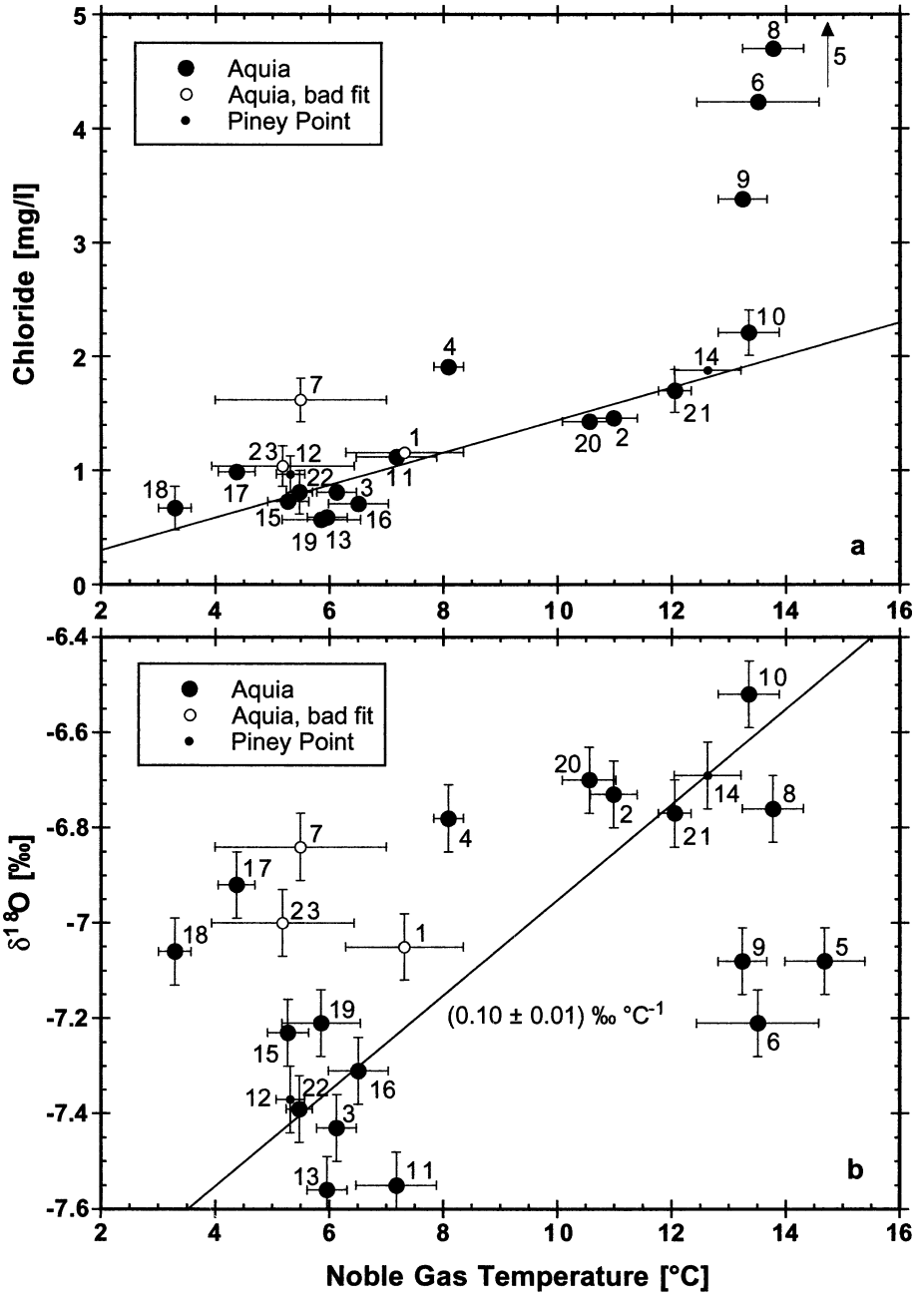

Fig. 6. Correlations of potential climate proxies with NGT. Meaning of symbols as in Figure 5. a) Chloride. Except for the outcrop wells (MD5, 6, 8, 9) with high chloride concentrations and to some extent the most downgradient well MD4, there is a good correlation between chloride and NGT ($r = 0.92$). b) $\delta^{18}O$. The correlation between $\delta^{18}O$ and NGT is blurred again by wells from the outcrop (MD5, 6, 9) and the downgradient well MD4, and in addition by wells MD17 and 18. Excluding these wells, two data clusters remain that define a good correlation ($r = 0.91$) with a slope of (0.10 ± 0.01) ‰°C^{-1}.

and NGT values (centered at about −7.4‰ and 6°C), and a "warm" one with higher $\delta^{18}0$ and NGT values (about −6.7‰ and 12°C). The wells that do not fit into this classification are partly the same as those excluded from the fit in Figure 6a: The downgradient well MD4, wells MD5, 6 and 9 from the recharge area, and the wells with the lowest NGTs, MD17 and 18. Unexpectedly low $\delta^{18}0$-values in the recharge area were also observed by Purdy (1991). Disregarding these wells, there seems to be a weak climate signal in the $\delta^{18}0$-data (slope (0.10 ± 0.01) ‰°C^{-1}, $r = 0.91$). Three climate related factors influencing the $\delta^{18}0$-values have to be taken into account: i) ice-volume effect; ii) continental effect; iii) temperature effect.

The ice-volume effect is due to the storage of isotopically depleted water in glacial ice sheets and led to a ≈1.3‰ increase

of the $\delta^{18}0$ of sea water during the LGM (Fairbanks, 1989). Assuming that samples with low NGTs are of Pleistocene age, their $\delta^{18}0$ values should be corrected by subtracting up to 1.3 ‰. If such a correction were applied to the "cold" cluster identified in Figure 6b, the relationship between $\delta^{18}0$ and NGT would become evident (slope (0.29 ± 0.03) ‰°C^{-1}, $r = 0.95$). However, reliable dating of the samples should be combined with a chronology of ice-volume changes to substantiate this correction.

The continental effect, i.e., the decrease of $\delta^{18}0$-values with distance from the coast (Rozanski et al., 1993), should have lowered the $\delta^{18}0$-values during the Pleistocene, when lower sea levels increased the distance of the Aquia outcrop from the coast, in analogy to the argument for chloride. Considering an inland gradient of -0.6‰/100 km as found in the Floridan aquifer (Atlantic Coastal Plain, Georgia) by Clark et al. (1997), and an increase of the distance to the coast by ~180 km during the LGM (Purdy et al., 1992), we estimate that the continental effect could have had a similar magnitude as the ice-volume effect.

The temperature effect may be estimated from a modern analog. The monitoring station of the IAEA/WMO network nearest to our study area is Hatteras (35.27°N, 75.55°W). Monthly mean values of $\delta^{18}0$ and temperature at this station are only weakly correlated ($r^2 = 0.13$) with a comparatively low slope of 0.09‰°C^{-1} (IAEA, 1992). Such weak $\delta^{18}0$-temperature relationships are typical for the Atlantic Coastal Plain region, as indicated by the data from other stations near the east coast of North America (IAEA, 1992), as well as isotope studies in coastal aquifers (Purdy, 1991; Plummer, 1993; Clark et al., 1997). The fact that the slope from Hatteras is close to the uncorrected $\delta^{18}O$/NGT slope of 0.1‰°C^{-1} between the two main clusters in Figure 6b may be fortuitous. A tentative interpretation of the data is that the sea-level related ice-volume and continental effects practically cancelled each other, and the remaining $\delta^{18}0$ signal indeed reflects a temperature effect similar to the modern $\delta^{18}0$-temperature relationship.

5.2. Chemical Evolution and ^{14}C ages

The ^{14}C ages calculated by using the Fontes and Garnier (1979) model (Table 2) indicate that all samples downstream of the outcrop area are of Pleistocene age, and most of them are older than 30 kyr. These ages seem to be inconsistent with several indications from the climate-sensitive variables. Most importantly, wells MD2, 10, 14, and 20, which according to NGT, chloride, and $\delta^{18}0$ (Fig. 6) appear to be of Holocene age, have ^{14}C ages between 17 and 32 kyr, clearly placing them into the Pleistocene. Also wells MD7 and 23, for which we have no NGT results but which are expected to be rather young on the basis of their location near the recharge area (Fig. 1), their high chloride concentrations (Fig. 3a) and $\delta^{18}0$-values (Fig. 4a), have ^{14}C ages of 15 and 18 kyr, respectively. A further problem is posed by wells MD15, 18, and 19, located at flow distances of 25 to 30 km. Their low NGTs and chloride concentrations seem to indicate an origin in the LGM, i.e., at ^{14}C ages of ~18 kyr. However, their ^{14}C activities below the detection limit (<0.4 pmc) imply ages >35 kyr independent of the model used to calculate the initial ^{14}C activity.

Obviously, the conventional interpretation of the carbon isotope data is inconsistent with the interpretation of NGTs, chloride concentrations, and stable isotopes as climate indicators. The ^{14}C activity minimum in the region of wells 15, 18, and 19 implies unusually low flow velocities along the flow lines that lead into this area. Such a scenario is not supported by hydrogeologic data (Chapelle and Drummond, 1983), as well as the quasi-linear increase of ^{4}He concentrations with flow distance, both indicating a rather uniform flow pattern. If we rely on the consistent picture provided by flow distance, ^{4}He, and the climate indicators rather than the modeled ^{14}C ages, we have to find an explanation for the depletion of ^{14}C in the center of our study area. Such an explanation could be unusually strong chemical and isotopic exchange processes along the flow paths leading to the low-^{14}C region that are not resolved by the models typically used for converting ^{14}C activities into ages.

The chemical and isotopic evolution of Aquia water including the processes influencing the carbon system in the Aquia aquifer have been discussed and modeled by Chapelle (1983), Chapelle and Drummond (1983), Chapelle and Knobel (1985), Plummer et al. (1994) and Appelo (1994). Their results can be summarized as follows:

1. In the recharge area, the meteoric water is transformed rapidly to the calcium-magnesium-bicarbonate water typical for region I by dissolution of magnesium-bearing shell material in the presence of soil-gas CO_2. The carbonate from the shell material has $\delta^{13}C$ and ^{14}C values close to zero due to its marine origin and high age, respectively. In contrast, the soil-gas CO_2 has a $\delta^{13}C$ value of about -25 ‰ and a ^{14}C value of 100 pmc, reflecting its recent biogenic origin.
2. Downgradient of the recharge area, but still in the 40 km wide region I, the water chemistry remains relatively constant, except for a slight increase in Mg^{2+} and parallel decrease in Ca^{2+}. These changes are due to further dissolution of magnesium-calcite and precipitation of calcite, as the water becomes saturated with respect to calcite. The precipitation of calcite explains the frequent occurrence of calcite cementation in this area (Chapelle, 1983).
3. In region II (~40 to 80 km from the recharge area), HCO_3^- remains relatively constant, whereas Na^+ rises and Ca^{2+} and Mg^{2+} decline. This is explained by a cation exchange reaction (Ca^{2+} and Mg^{2+} exchanged for Na^+) with glauconite acting as the exchange medium.
4. In region III (more than 80 km from the outcrop) HCO_3^- and Na^+ increase rapidly, whereas Ca^{2+} and Mg^{2+} remain low. This is explained by dissolution of magnesium-calcite in the presence of biogenic CO_2 and concurrent cation exchange (Chapelle and Knobel, 1985), or by proton exchange in the course of freshening of the aquifer (Appelo, 1994).

The first step can be seen in our samples from the outcrop. Wells MD5, 8 and 9 yielded very acidic water due to the presence of soil-gas CO_2. Furthermore, these wells exhibit low Ca^{2+} and Mg^{2+} concentrations (Fig. 3b), low $\delta^{13}C$ values and high ^{14}C activities (Fig. 4b). In well MD6, which lies still within the outcrop area and has a $^{3}H/^{3}He$ age of 25 yr, the pH has neutralized, the Ca^{2+} concentration has risen to a maximum (Fig. 3b), $\delta^{13}C$ has increased to -9.1 ‰ and ^{14}C activity has dropped to 28 pmc (Fig. 4b). The change in carbon isotopic composition in this first step can be described by the model of Fontes and Garnier (1979), which yields an initial ^{14}C activity

of 36 pmc for well MD6, reasonably close to the observed value.

Most of the wells used in this study are located in the confined part of region I, where the second step of the above described chemical evolution takes place. Since the changes in Mg^{2+} and Ca^{2+} concentrations in this region are rather small (Fig. 3b), relatively little dissolution and re-precipitation of carbonate is needed to satisfy mass balance. Little recrystallization of calcite and hence little isotope exchange is also in accordance with the observed practically constant $\delta^{13}C$. The dramatic decrease of ^{14}C activity from 28 pmc at well MD6 to 1.8 pmc at well MD20 and further to values below the detection limit at wells MD15, 18 and 19 (Fig. 4b) therefore appears to indicate very high ages. For instance, if 28 pmc is taken as initial ^{14}C activity and no isotopic exchange is assumed, apparent ages of 23 kyr for well MD20 and 47 kyr for the wells with ^{14}C values of 0.1 pmc are obtained. These first order calculations are not significantly changed if we use the program NETPATH with a reaction scheme including isotope exchange by calcite recrystallization (Plummer et al., 1994) to model the ^{14}C evolution.

However, the ^{14}C ages obtained with this model appear unrealistically high for all wells in this region except well MD2, which represents the most southerly flow line (Fig. 1). The relatively high ^{14}C value of 3.8 pmc at well MD2 offers an explanation for the non-zero ^{14}C values at flow distances of 50 km and greater, despite the results below the detection limit observed at ~30 km distance. The wells at great flow distances in southern Calvert County receive water from flow lines that pass through well MD2 or further south (Fig. 1). In this southern part, the ^{14}C ages calculated using the model of Fontes and Garnier (1979) (Table 2) are more consistent with expectations from chloride and noble gases. It seems that along the northern flow lines passing from Prince Georges County to northern Calvert County the ^{14}C activities are reduced by an isotope exchange process in addition to that needed to satisfy mass and isotope balance.

Plummer et al. (1994) tested several models for the carbon isotope evolution in the Aquia aquifer. Their favored model includes proton exchange and calcite dissolution, as proposed by Appelo (1994). A much stronger reduction of ^{14}C can be achieved in another scenario, which includes carbon isotope exchange with the carbonate minerals. Both models explain the isotopic and chemical changes observed in region III of the Aquia aquifer, in particular the increases of $\delta^{13}C$, Na^+, and HCO_3^-. Howerver, we are looking for an explanation for very low ^{14}C values in parts of region I, where $\delta^{13}C$, Na^+, and HCO_3^- are approximately constant. Incongruent dissolution of marine calcite could explain the data except for $\delta^{13}C$, which should increase towards the source value of ~0 ‰ (e.g., Wigley et al., 1978). A source of old (^{14}C free) carbon with a $\delta^{13}C$ value close to that of region I water (about −11‰) appears to be required to satisfy all constraints. Such a source could be the calcite cementation beds, which are a characteristic feature of the region with low ^{14}C activities.

It has been shown based on mass balance considerations (Chapelle, 1983) and isotopic data (Chapelle and Knobel, 1985) that calcite cementation is of secondary origin, i.e., due to calcite precipitation from the groundwater. Chapelle and Knobel (1985) reported $\delta^{13}C$ values ranging from −10.4 to −2.2‰ for the calcite cement, and from −0.6 to + 1.9‰ for the shell material. An evolution of groundwater $\delta^{13}C$ values towards the isotopic composition of the calcite cements (increasing with flow distance from −8.8 to −3.9‰) has been observed in another Coastal Plain aquifer (McMahon and Chapelle, 1991). If the calcite cement had $\delta^{13}C$ values similar to those of the groundwater in region I, isotope exchange of the DIC with the calcite cement by incongruent dissolution would affect only the ^{14}C activity of the DIC, but not the $\delta^{13}C$ values. NETPATH simulations showed that calcite exchange of several mmol l^{-1} could lower the ^{14}C activity to such an extent that values below 0.4 pmc are consistent with ages of the order of 20 kyr.

The disadvantage of the proposed explanation of the low ^{14}C activities is that it cannot be tested independently, since the exchange affects no other parameters. The lack of constraints on the amount of calcite that was exchanged renders ^{14}C useless as dating tool. The same situation was encountered by Andrews et al. (1994) in an aquifer in Niger. These authors stressed that such an exchange with secondary calcite deposits can occur if the groundwater is saturated with respect to calcite. In the Aquia aquifer, our data as well as the literature (e.g., Chapelle, 1983) confirm that calcite saturation is reached in the region of high calcite cementation. Very low ^{14}C activities due to strong interaction with the aquifer material were also found in the Floridan aquifer in Georgia (Clark et al., 1997; Plummer, 1993), which is also situated in the Atlantic Coastal Plain.

In their study of the Black Creek aquifer in South Carolina, also in the Coastal Plain, McMahon and Chapelle (1991) found no evidence for dissolution of secondary low-Mg calcite cement, which is thermodynamically more stable than shell material. This observation argues against our assumption of calcite cement recycling. McMahon and Chapelle (1991) favored a model for the evolution of carbonates in the Black Creek aquifer that includes addition of organic and inorganic carbon from confining beds, dissolution of shell material, and precipitation of calcite cement. The isotopic balance can be closed in this model by the addition of organic carbon with low $\delta^{13}C$. Similar processes may also be responsible for the ^{14}C depletion in the Aquia aquifer. Only very sophisticated modeling of the geochemical evolution of the Aquia groundwater along different flow lines offers a chance to derive reliable ^{14}C ages. Such modeling is beyond the scope of this study and probably not possible based on the available data. Moreover, for those wells with ^{14}C activities below the detection limit, any attempt to derive accurate ^{14}C ages is futile.

Regions II and III of Chapelle (1983) (steps 3 and 4 in the evolution as described above) are not very well represented in this study. The general chemical and isotopic evolution observed in the wells at flow distances greater than 40 km is consistent with the models described in the literature.

5.3. He-Ages

He concentrations often increase with groundwater age due to accumulation of radiogenic He produced by α-decay of U and Th series nuclides in crustal minerals (e.g., Andrews and Lee, 1979; Torgersen and Clarke, 1985; Stute et al., 1992b; Solomon et al., 1996). There are three potential sources of radiogenic He in groundwater: i) in situ production within the

Table 6. Results of U, Th, and Li analyses on two cores.

Core	Depth [m]	Formation	U [μg/g]	Th [μg/g]	Li [μg/g]
CH-Bf148	74.1	Marlboro	2.72 ± 0.01	16.19 ± 0.16	372 ± 24
CH-Bf148	83.5	Aquia	1.07 ± 0.03	1.81 ± 0.01	21.7 ± 0.5
CH-Bf148	100.6	Aquia	0.91 ± 0.01	3.50 ± 0.03	17.4 ± 0.3
CH-Bf148	112.8	Aquia	1.39 ± 0.01	5.06 ± 0.03	26.8 ± 0.7
CH-Bf148	121.8	Brightseat	2.07 ± 0.01	6.07 ± 0.02	46.2 ± 1.7
PG-Df35	14.9	Marlboro	2.41 ± 0.03	14.67 ± 0.04	439 ± 40
PG-Df35	21.9	Aquia	1.43 ± 0.01	5.82 ± 0.02	27.7 ± 0.2
PG-Df35	36.6	Aquia	1.02 ± 0.01	2.84 ± 0.02	12.0 ± 0.1
PG-Df35	54.3	Aquia	1.40 ± 0.01	4.62 ± 0.03	14.6 ± 0.2

aquifer matrix; ii) release of stored He from fresh sediments; and iii) a flux from adjacent layers or even the whole underlying crust. The rate of He accumulation due to the first source can be estimated if U and Th concentrations of the aquifer material are known. However, the strength of the two other sources can vary by orders of magnitude depending on the geological setting. Therefore, He accumulation in ground water typically provides only a qualitative timescale.

The He excesses found in the Aquia aquifer are remarkably small in view of the presumed groundwater age (Fig. 5b). A rough calculation with a typical in situ production rate of 5×10^{-12} cm^{3}STP g^{-1} yr^{-1} (Torgersen and Clarke, 1985) shows that in situ production alone has the right order of magnitude to explain the observed excess. Significant release of stored He from the sediment is not expected because of the Paleocene age of the Aquia formation. An explanation for the absence of a considerable crustal He flux could be that the underlying Magothy aquifer flushes the He out of the system before it can migrate across it and reach the Aquia aquifer. This explanation is consistent with the high He excess in well MD4, because the Magothy is absent at this location (Fig. 2). If the hypothesis of practically pure in situ production holds true for the other wells, quantitative dating should be possible.

The ^{4}He accumulation rate A_{He} due to in situ production can be calculated as follows (Stute et al., 1992b, modified from Andrews and Lee, 1979):

$$A_{He} = \Lambda_{He} \frac{\rho_r}{\rho_w} (C_U \cdot P_U + C_{Th} \cdot P_{Th}) \cdot \frac{1 - n}{n_{eff}} \qquad (2)$$

The release factor Λ_{He} (fraction of produced ^{4}He which is released from minerals into the water) is usually taken to be 1 (e.g., Andrews and Lee, 1979; Torgersen and Clarke, 1985). The density of the aquifer material ρ_{rock} is taken as 2.6 g cm^{-3} for the predominant quartz sand. The ^{4}He production rates from U and Th decay are $P_U = 1.19 \cdot 10^{-13}$ cm^{3}STP μg_U^{-1} yr^{-1} and $P_{Th} = 2.88 \cdot 10^{-14}$ cm^{3}STP μg_{Th}^{-1} yr^{-1} (Andrews and Lee, 1979). The U and Th concentrations (C_U, C_{Th}) and the total and effective porosity (n, n_{eff}) of the aquifer matrix have to be measured.

Samples of the Aquia sand were obtained from two cores from the northwestern part of the study area (Fig. 1), stored by the Maryland Geological Survey. The cores have been described in detail by Hansen (1977), and Wilson and Fleck (1990). Concentrations of U, Th and Li in six samples of the aquifer material and three samples of the the adjacent aquitards (Table 6) were determined by isotope dilution ICP-MS following the procedures described by Zheng (1999). The U concentrations in the Aquia sand range from 0.9 to 1.4 μg g^{-1} with a mean value of (1.20 ± 0.09) μg g^{-1}. The Th concentrations are more variable, ranging from 1.8 to 5.8 μg g^{-1} with a mean value of (3.9 ± 0.6) μg g^{-1}. The mean Li concentration is (20 ± 3) μg g^{-1}. The concentrations in the aquitards are higher, particularly in the overlying Marlboro clay (mean values 2.56 μg g^{-1} for U, 15.4 μg g^{-1} for Th, and 406 μg g^{-1} for Li). The total porosity n as well as the effective porosity n_{eff} were measured by Hansen (1977) on 10 Aquia samples from one of the above and a different core, yielding mean values of (0.39 ± 0.02) for n and (0.25 ± 0.02) for n_{eff}. The few available data for the aquitards are similar.

With the above mean values, Eqn. 2 yields a He accumulation rate of $(1.6 \pm 0.2) \cdot 10^{-12}$ cm^{3}STP g^{-1} yr^{-1} for the Aquia aquifer. The resulting He ages (Table 5) have a nominal uncertainty of about ±14%, mostly due to the error of the accumulation rate. However, their reliability depends on the validity of the assumption of pure in situ production. The He ages may be interpreted as maximum estimates, because an additional He flux from adjacent aquitards or deeper layers of the crust could be present.

The isotope ratio may be used to discern different sources of the accumulated He. Although a detailed knowledge of the sediment composition would be required for a precise calculation of the ^{3}He/^{4}He production ratio, rough estimates can be made on the basis of the measured Li concentrations (Table 6) and the calculations made by Andrews (1985) for various rock matrices. We estimate ^{3}He/^{4}He production ratios of less than 10^{-8} for the Aquia sand, 1 to $2 \cdot 10^{-8}$ for the Brightseat formation, and more than 10^{-7} for the Marlboro clay. Since the data from well MD4 yield an upper limit of $1.8 \cdot 10^{-8}$ for the radiogenic ^{3}He/^{4}He ratio in the Aquia, a major contribution of He produced in the Marlboro clay can be ruled out. Nevertheless, some He diffusion from the aquitards into the aquifer appears likely, given that the U and Th concentrations in the aquitards are about two to three times higher.

The He ages generally correlate well with the estimated flow distance (compare Fig. 5b). Excluding the four most downgradient wells (MD10 —too young in all parameters, MD12 and 14 —Piney Point, MD4 —possibly influenced by crustal He flux), a linear regression yields a mean groundwater flow velocity of (0.7 ± 0.1) m yr^{-1} for flow distances between ~10 and 50 km. If the He ages are maximum estimates, this result

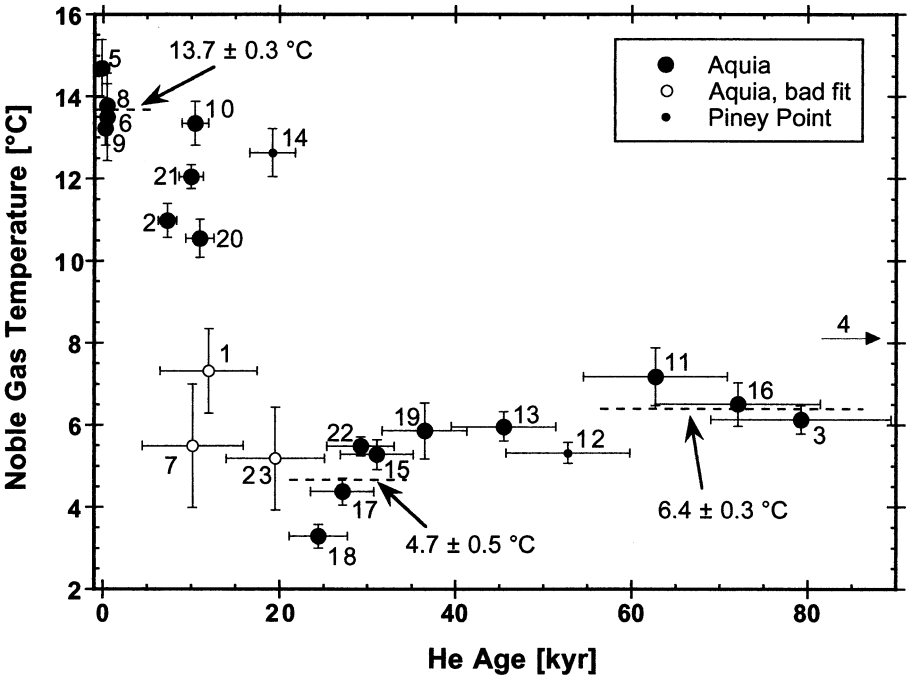

Fig. 7. Noble gas temperatures as a function of the He accumulation age. Meaning of symbols as in Figure 5. The He ages based on in situ production are valid only for the Aquia samples and most likely represent upper limits to the true ages. Three groups of wells are identified: The outcrop wells (MD5, 6, 8, 9) clearly represent modern (Holocene) climate conditions. The wells MD15, 17, 18, and 22 are thought to best represent the LGM, whereas wells MD3, 11, and 16 seem to originate from an earlier part of the LGP. The other wells may reflect climatic transitions and are not used in the calculation of mean NGTs for the defined climate states. A difference of (9.0 ± 0.6) °C is obtained for the LGM-Holocene transition, whereas during the LGP in general the temperature seems to have been (7.3 ± 0.5) °C colder than at present.

represents a lower limit for the true flow velocity. It is considerably smaller than the estimates discussed by Purdy et al. (1992), which range between 2.6 and 4 m yr^{-1}. Yet, the even lower flow velocity of 0.2 m yr^{-1} inferred from ^{36}Cl by Purdy et al. (1996) for flow distances larger than 50 km is in reasonable agreement with the high apparent He age at well MD4.

5.4. Holocene - LGM Temperature Difference

To quantify the temperature difference between the Holocene and the LGM, we have to identify the samples representing these two climate states. This identification is primarily based on the time scale provided by the He age (Fig. 7), although the absolute ages are quite uncertain. Further indications on the age of the water can be obtained from flow distance, chloride, ^{14}C, and tritium. Because He age and flow distance are not properly defined for the Piney Point aquifer, wells MD12 and 14 are not used in the following discussion, although the climate indicators (Fig. 6) suggest that they represent the two main climate states.

Tritium concentrations and $^{3}He/^{4}He$ ratios clearly show that the water of the four shallow wells in the outcrop region of the Aquia (wells MD5, 6, 8, 9) has infiltrated during the last few decades. This classification as young samples is also supported by the He ages, as well as the high ^{14}C activities and chloride concentrations. Based on their He ages of around 10 kyr, wells MD1, 2, 7, 10, 20, and 21 might also contain water of Holocene age. No reliable NGTs could be determined for wells MD1 and 7. Wells MD2 and MD10 are located at large flow distances where older water would be expected. Wells MD20 and 21 are located close to the outcrop area, but the ^{14}C-activity at well MD20 is rather low with 1.8 pmc (unfortunately, the ^{14}C sample for MD21 was lost). Thus, none of these samples can clearly be classified as purely of Holocene age, some may be affected by mixing or represent the transition between LGM and Holocene.

Hence, the estimate of the Holocene temperature is entirely based on NGTs from the outcrop wells (MD5, 6, 8, 9), which yield values between 13.2 and 14.7°C. The weighted mean NGT for these modern groundwaters is (13.7 ± 0.3) °C. The 1921 to 1970 average of the mean annual air temperatures from five stations (Karl et al., 1990) in or near the outcrop area is 12.8°C. According to Smith et al. (1964), ground temperatures in the temperate United States are on average 1 ± 1°C higher than mean annual air temperatures. Hence the measured NGTs of the outcrop wells appear to represent modern ground temperatures.

Identification of the wells representing LGM conditions is more difficult. The peak of the LGM is commonly assumed to have occurred at ~18,000 ^{14}C years or 21,000 calendar years BP. Keeping in mind that the ^{14}C ages listed in Table 2 are most likely too high due to unaccounted carbonate exchange processes and that the He ages given in Table 5 are possibly overestimated due to unaccounted external He sources, we may tolerate somewhat higher He ages and considerably higher ^{14}C

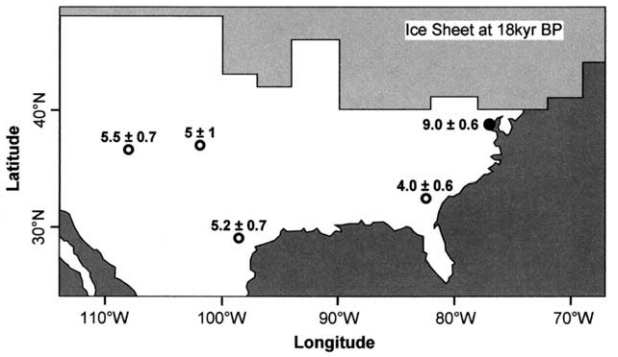

Fig. 8. LGM-Holocene temperature changes derived from NGT records in North America. The temperature change of 9.0°C found at our study site is clearly larger than the results from previous noble gas studies in the USA: New Mexico: 5.5°C (Stute et al., 1995a), Colorado: 5°C (Clark et al., 1998), Texas: 5.2°C (Stute et al., 1992a), Georgia: 4°C (Clark et al., 1997). The extension of the ice sheet at 18 kyr BP is shown for comparison (Peltier, 1994).

ages. Wells MD15, 17, 18, and 22, located between 26 and 38 km from the outcrop, have He ages between 24 and 31 kyr and chloride concentrations below 1 mg l^{-1}. We believe that these wells are the most likely candidates for water from the LGM, despite their low ^{14}C activities and correspondingly high apparent ^{14}C ages (>33 kyr). Additional candidates may be wells MD13 and 19, which also have low chloride concentrations but somewhat higher He ages (45 and 36 kyr, respectively). Well MD23 with a He age of 20 kyr has an NGT that was judged unreliable because of a bad fit of the noble gas concentrations. The four presumed LGM samples (MD15, 17, 18, 22) yield NGTs between 3.3 and 5.5°C, with a weighted mean NGT of (4.7 ± 0.5) °C. Inclusion of wells MD13 and 19 would increase the mean NGT slightly to 4.9°C.

The difference between the best estimates for the NGTs of the Holocene and LGM is (9.0 ± 0.6)°C. Within the errors, this result for the Holocene - LGM temperature change is identical to the value of 8.6°C derived from groundwater in Hungary (Stute and Sonntag, 1992). It is considerably larger than previous estimates from noble gas studies in North America (Stute et al., 1992a, 1995a; Clark et al., 1997, 1998), which all indicated a glacial cooling of ~5°C (Fig. 8). Of particular interest are recharge temperature records from the Floridan aquifer in Georgia, which represents a very similar setting in the Atlantic Coastal Plain, but lies ~7° latitude or 800 km further to the south. In this aquifer, Plummer (1993) found a mean difference of (5.3 ± 2.5) °C between Ar-N_2 recharge temperatures of glacial and interglacial samples from several areas, whereas the complete noble gas data set from two flowlines of Clark et al. (1997) yielded a glacial cooling of (4.0 ± 0.6) °C. These findings indicate that the *N*-S temperature gradient between 32 and 39°N in eastern North America was much stronger during the LGM than it is at present.

The large Holocene —LGM temperature difference at our study site is probably due to the influence of the Laurentide ice sheet, which at its maximum extension reached as close as 250 km to the study site (using the ice-sheet reconstruction of Peltier, 1994). Climate models (Manabe and Broccoli, 1985; COHMAP, 1988; Bartlein et al., 1998) indicate major reorganizations of the circulation over North America in response to the Laurentide ice sheet, in particular a southward displacement or even a split of the jet stream and the development of a glacial anticyclone over the ice sheet. As a result, the models yield very cold temperatures over and adjacent to the ice sheet and a larger than present temperature gradient south of the ice sheet.

Cold temperatures close to the margin of the Laurentide ice sheet and a steeper north-south temperature gradient are also indicated by paleoclimate reconstructions based on pollen, plant macrofossil, and midge larvae records in lake sediments (Webb III et al., 1998; Jackson et al., 2000; Levesque et al., 1997). With regard to our study site, the pollen-based reconstruction of Webb III et al. (1998) suggests ≈15°C lower January temperatures and ≈5°C lower July temperatures than today. The more recent analysis of Jackson et al. (2000) indicates even colder January temperatures (≈22°C lower than present). The paleoclimate simulations of Bartlein et al. (1998) yield a similar pattern of ≈20°C lower January temperatures and ≈5°C lower July temperatures, with an annual mean LGM cooling for the entire southeastern US of 10°C. The model of Crowley and Baum (1997) yielded a LGM cooling of 9.4°C for our study site, in very good agreement with our result.

In summary, our value of 9°C cooling at the LGM lies at the lower end of the estimates for the region. In particular, our data suggest a somewhat weaker cooling than the recent synthesis of vegetation data of Jackson et al. (2000). Weaknesses of both methods may explain the difference. Problems of vegetation reconstructions are missing modern analogues and the influence of temperature-independent environmental changes, in particular of the atmospheric CO_2 level. The noble gas method may underestimate the LGM-Holocene temperature change because of several reasons: i) dispersive groundwater flow smooths out climate extremes (Stute and Schlosser, 1993, 2000); ii) the coldest periods may be under-represented in the groundwater archive because frozen ground may have prevented infiltration (Stute and Sonntag, 1992; Beyerle et al., 1998); iii) the difference between the ground temperature measured by the noble gas thermometer and the mean annual air temperature may have been larger during the LGM due to the insulating effect of snow cover (Smith et al., 1964) or because of lower water tables in the recharge area in response to lower sea level.

In addition to the LGM, the preceding climate state of the LGP may also be represented in our data. Water clearly older than the LGM is found in wells MD3, 11, and 16, which have He ages between 60 and 80 kyr and are located at flow distances of ~50 km. Well MD4, with its high He age of 280 kyr, may be even older than the LGP. The NGTs from the presumed LGP wells (MD3, 11, 16) vary between 6.1 and 7.2°C, with a weighted mean of (6.4 ± 0.3) °C. Inclusion of wells MD13 and 19 would slightly lower the mean to 6.2°C. Hence, it appears that during at least a part of the LGP, which we cannot precisely date, the mean annual temperatures were about (7.3 ± 0.5) °C colder than during the Holocene.

6. CONCLUSIONS

Our ^{14}C and noble gas data from the Aquia aquifer in southeastern Maryland clearly confirm the presence of paleowater in this formation. The correlation between NGTs and

chloride concentrations support the interpretation of chloride variations as reflecting past sea-level changes, and indicates that the wells at flow distances of 25 to 40 km may tap water that infiltrated at times around the LGM. This interpretation is not confirmed, however, by ^{14}C ages derived with the standard models used for calculation of the initial ^{14}C activity. The literature on the geochemistry of the Aquia and other Atlantic Coastal Plain aquifers suggests that incongruent dissolution of carbonates is an active process at least in parts of these aquifers, associated with the presence of secondary calcite cementation. Exchange of carbon between the solid and dissolved phase by dissolution and precipitation can in principle explain the unexpectedly low observed ^{14}C activities. However, it seems impossible to accurately correct for such exchange processes based on the available data.

In return, the Aquia aquifer appears to be exceptionally well suited for the use of radiogenic He as a quantitative dating tool. The observed He concentrations are so low that they can be explained by accumulation of purely in situ produced radiogenic He. From concentrations of U and Th and porosities measured on drill cores from the Aquia, a ^4He accumulation rate of $(1.6 \pm 0.2) \cdot 10^{-12}$ $cm^3STP\ g^{-1}\ yr^{-1}$ was calculated. This rate can be used to convert calculated radiogenic He excesses into groundwater residence times.

The interpretation of the measured noble gas concentrations in terms of NGTs and He ages requires a correct description of the excess air component. The assumption of excess air formation by partial dissolution of entrapped air (Aeschbach-Hertig et al., 2000) explains most measured noble gas concentrations within experimental accuracy and yields consistent results for the radiogenic He component.

The calculated NGTs and He ages indicate that mean annual ground temperatures in Maryland were (9.0 ± 0.6) °C lower during the LGM than at present. This temperature difference clearly exceeds previous noble gas results from North America and indicates a steeper *N*-S temperature gradient during the LGM compared to the present. These findings are ascribed to the proximity (250 km) of the Laurentide ice sheet during the LGM. A cooling of 9.0°C in Maryland during the LGM is at the lower end of estimates derived from pollen data. It is possible that the noble gas paleothermometer slightly overestimates the LGM mean annual temperatures because of reduced infiltration and/or enhanced difference between ground and air temperatures during the coldest periods.

Acknowledgments—We thank D. L. Bropst of the Calvert County Dept. of Public Works as well as numerous private well owners for letting us sample their wells, H. J. Hansen of the Maryland Geological Survey for giving us access to Aquia sediment cores, M. C. Castro for performing U and Th analyses on the core samples, and L. N. Plummer and K. Rozanski for careful and constructive reviews. W. Aeschbach-Hertig was supported by a fellowship of the Swiss National Science Foundation. R. F. Reuter was supported by the Maryland Water Resources Research Center. The LDEO noble gas facility was supported by NSF and the W. M. Keck Foundation. LDEO contribution 6242.

Associate editor: D. E. Fisher

REFERENCES

Aeschbach-Hertig W., Peeters F., Beyerle U. and Kipfer R. (1999) Interpretation of dissolved atmospheric noble gases in natural waters. *Water Resour. Res.* **35,** 2779–2792.

Aeschbach-Hertig W., Peeters F., Beyerle U. and Kipfer R. (2000) Palaeotemperature reconstruction from noble gases in ground water taking into account equilibration with entrapped air. *Nature* **405,** 1040–1044.

Aeschbach-Hertig W., Beyerle U., Holocher J., Peeters F. and Kipfer R. (2001). Excess air in groundwater as a potential indicator of past environmental changes. In *International Conference on the Study of Environmental Change Using Isotope Techniques* IAEA-CN-80/29, pp. 34–36. IAEA, Vienna.

Andrews J. N. (1985) The isotopic composition of radiogenic helium and its use to study groundwater movement in confined aquifers. *Chem. Geol.* **49,** 339–351.

Andrews J. N. and Lee D. J. (1979) Inert gases in groundwater from the Bunter Sandstone of England as indicators of age and palaeoclimatic trends. *J. Hydrol.* **41,** 233–252.

Andrews J. N., Goldbrunner J. E., Darling W. G., Hooker P. J., Wilson G. B., Youngman M. J., Eichinger L., Rauert W. and Stichler W. (1985) A radiochemical, hydrochemical and dissolved gas study of groundwaters in the Molasse basin of Upper Austria. *Earth Planet. Sci. Lett.* **73,** 317–332.

Andrews J. N., Fontes J.-C., Aranyossy J.-F., Dodo A., Edmunds W. M., Joseph A. and Travi Y. (1994) The evolution of alkaline groundwaters in the continental intercalaire aquifer of the Irhazer Plain, Niger. *Water Resour. Res.* **30,** 45–61.

Appelo C. A. J. (1994) Cation and proton exchange, pH variations, and carbonate reactions in a freshening aquifer. *Water Res. Res.* **30,** 2793–2805.

Ballentine C. J. and Hall C. M. (1999) Determining paleotemperature and other variables by using an error-weighted, nonlinear inversion of noble gas concentrations in water. *Geochim. Cosmochim. Acta.* **63,** 2315–2336.

Bartlein P. J., Anderson K. H., Anderson P. M., Edwards M. E., Mock C. J., Thompson R. S., Webb R. S., Webb III T. and Whitlock C. (1998) Paleoclimate simulations for North America over the past 21,000 years: Features of the simulated climate and comparison with paleoenvironmental data. *Quat. Sci. Rev.* **17,** 549–585.

Beyerle U., Purtschert R., Aeschbach-Hertig W., Imboden D. M., Loosli H. H., Wieler R. and Kipfer R. (1998) Climate and groundwater recharge during the last glaciation in an ice-covered region. *Science.* **282,** 731–734.

Chapelle F. H. (1983) Groundwater geochemistry and calcite cementation of the Aquia aquifer in southern Maryland. *Water Resour. Res.* **19,** 545–558.

Chapelle F. H. and Drummond D. D. (1983) Hydrogeology, digital simulation, and geochemistry of the Aquia and Piney Point-Nanjemoy aquifer system in southern Maryland. *Report of Investigations* **No. 38,** Maryland Geological Survey.

Chapelle F. H. and Knobel L. L. (1985) Stable carbon isotopes of HCO_3 in the Aquia Aquifer, Maryland: Evidence for an isotopically heavy source of CO_2. *Ground Water.* **23,** 592–599.

Clark J. F., Stute M., Schlosser P., Drenkard S. and Bonani G. (1997) A tracer study of the Floridan aquifer in southeastern Georgia: Implications for groundwater flow and paleoclimate. *Water Resour. Res.* **33,** 281–289.

Clark J. F., Davisson M. L., Hudson G. B. and Macfarlane P. A. (1998) Noble gases, stable isotopes, and radiocarbon as tracers of flow in the Dakota aquifer, Colorado and Kansas. *J. Hydrol.* **211,** 151–167.

Clarke W. B., Jenkins W. J. and Top Z. (1976) Determination of tritium by mass spectrometric measurement of ^3He. *Int. J. Appl. Rad. Iso.* **27,** 515–522.

Clever H. L. (1979) (ed.) Krypton, xenon and radon - gas solubilities. In *Solubility data series* Vol. 2, pp. 357. International Union of Pure and Applied Chemistry, Pergamon Press, Oxford.

CLIMAP Project Members. (1976) The surface of the ice-age Earth. *Science.* **191,** 1131–1137.

CLIMAP Project Members. (1981) Seasonal reconstruction of the Earth's surface at the last glacial maximum. Map and Chart Series MC-36, Geol. Soc. Am., Boulder, Colorado.

COHMAP Project Members. (1988) Climatic changes of the last 18,000 years: Observations and model simulations. *Science.* **241,** 1043–1052.

Colinvaux P. A., Deoliveira P. E., Moreno J. E., Miller M. C. and Bush

M. B. (1996) A long pollen record from lowland amazonia: Forest and cooling in glacial times. *Science.* **274,** 85–88.
Crowley T. J. (2000) CLIMAP SSTs re-revisited. *Clim. Dyn.* **16,** 241–155.
Crowley T. J. and Baum S. K. (1997) Effect of vegetation on an ice-age climate model simulation. *J. Geophys. Res.* **102,** 16463–16480.
Cuffey K. M., Clow G. D., Alley R. B., Stuiver M., Waddington E. D. and Saltus R. W. (1995) Large arctic temperature change at the Wisconsin-Holocene glacial transition. *Science.* **270,** 455–458.
Fairbanks R. G. (1989) A 17,000-year glacio-eustatic sea level record: influence of glacial melting rates on the Younger Dryas event and deep-ocean circulation. *Nature.* **342,** 637–642.
Farrera I., Harrison S. P., Prentice I. C., Ramstein G., Guiot J., Bartlein P. J., Bonnefille R., Bush M., Cramer W., von Grafenstein U., Holmgren K., Hooghiemstra H., Hope G., Jolly D., Lauritzen S. E., Ono Y., Pinot S., Stute M. and Yu G. (1999) Tropical climates at the Last Glacial Maximum: a new synthesis of terrestrial palaeoclimate data. I. Vegetation, lake levels and geochemistry. *Clim. Dyn.* **15,** 823–856.
Fayer M. J. and Hillel D. (1986) Air encapsulation: 1. Measurement in a field soil. *Soil Sci. Soc. Am. J.* **50,** 568–572.
Fontes J.-C. and Garnier J.-M. (1979) Determination of the initial ^{14}C activity of the total dissolved carbon: A review of the existing models and a new approach. *Water Resour. Res.* **15,** 399–413.
Hansen H. J. (1974) Sedimentary facies of the Aquia formation in the subsurface of the Maryland Coastal Plain. Report of Investigations No. 21, Maryland Geological Survey.
Hansen H. J. (1977) Geologic and hydrologic data from two core holes drilled through the Aquia formation (eocene-paleocene), in Prince George's and Queen Anne's counties, Maryland. Open File Report. 77–02–1. Maryland Geological Survey.
Heaton T. H. E. and Vogel J. C. (1981) "Excess air"in groundwater. *J. Hydrol.* **50,** 201–216.
IAEA. (1992) Statistical treatment of data on environmental isotopes in precipitation. Technical Reports Series 331, International Atomic Energy Agency, IAEA.
Ingerson E. and Pearson F. J. (1964) Estimation of age and rate of motion of groundwater by the ^{14}C-method. In *Recent Researches in the Fields of Atmosphere, Hydrosphere and Nuclear Geochemistry,* pp. 263–283. Nagoya University, Nagoya, Japan.
Jackson S. T., Webb R. S., Anderson K. H., Overpeck J. T., Webb III T., Williams J. W. and Hansen B. C. S. (2000). Vegetation and environment in Eastern North America during the Last Glacial Maximum. *Quat. Sci. Rev.* **19,** 489–508.
Johnsen S. J., Clausen H. B., Dansgaard W., Fuhrer K., Gundestrup N., Hammer C. U., Iversen P., Jouzel J., Stauffer B. and Steffensen J. P. (1992) Irregular glacial interstadials recorded in a new Greenland ice core. *Nature.* **359,** 311–313.
Johnsen S. J., Dahl-Jensen D., Dansgaard W. and Gundestrup N. (1995) Greenland palaeotemperatures derived from GRIP bore hole temperature and ice core isotope profiles. *Tellus.* **47B,** 624–629.
Karl T. R., Williams C. N., Jr, Quinlan F. T. and Boden T. A. (1990) United States Historical Climatology Network (HCN) Serial Temperature and Precipitation Data. Publication No. 3404. Environmental Science Division, Carbon Dioxide Information and Analysis Center, Oak Ridge National Laboratory.
Levesque A. J., Cwynar L. C. and Walker I. R. (1997) Exceptionally steep north-south gradients in lake temperatures during the last deglaciation. *Nature.* **385,** 423–426.
Ludin A., Wepperning R., Bönisch G. and Schlosser P. (1997) Mass spectrometric measurement of helium isotopes and tritium in water samples. Technical Report, Lamont-Doherty Earth Observatory.
Mamyrin B. A. and Tolstikhin I. N. (1984) *Helium isotopes in nature.* Elsevier, Amsterdam, Oxford, New York, Tokyo
Manabe S. and Broccoli A. J. (1985) The influence of continental ice sheets on the climate of an ice age. *J. Geophys. Res.* **90,** 2167–2190.
McMahon P. B. and Chapelle F. H. (1991) Geochemistry of dissolved inorganic carbon in a Coastal Plain aquifer. 2. Modeling carbon sources, sinks, and $\delta^{13}C$ evolution. *J. Hydrol.* **127,** 109–135.
Peltier W. R. (1994) Ice age paleotopography. *Science.* **265,** 195–201.
Plummer L. N. (1993) Stable isotope enrichment in paleowaters of the southeast Atlantic Coastal Plain, United States. *Science.* **262,** 2016–2020.
Plummer L. N., Prestemon E. C. and Parkhurst D. L. (1994) An interactive code (NETPATH) for modeling net geochemical reactions along a flow path, version 2.0. Water-Resources Investigations Report, 94–4169. U.S. Geological Survey.
Press W. H., Flannery P. F., Teukolsky S. A. and Vetterling W. T. (1986) *Numerical Recipes.* Cambridge University Press, Cambridge.
Purdy C. B. (1991) Isotopic and chemical tracer studies of ground water in the Aquia Formation, southern Maryland: Including ^{36}Cl, ^{14}C, ^{18}O and ^{3}H. Ph. D. thesis, University of Maryland, College Park.
Purdy C. B., Burr G. S., Rubin M., Helz G. R. and Mignerey A. C. (1992) Dissolved organic and inorganic ^{14}C concentrations and ages for coastal plain aquifers in southern Maryland. *Radiocarbon.* **34,** 654–663.
Purdy C. B., Helz G. R., Mignerey A. C., Kubik P. W., Elmore D., Sharma P. and Hemmick T. (1996) Aquia aquifer dissolved Cl^- and $^{36}Cl/Cl$: Implications for flow velocities. *Water Resour. Res.* **32,** 1163–1171.
Roberts M. L., Bench G. S., Brown T. A., Caffee M. W., Finkel R. C., Freeman S. P. H. T., Hainsworth L. J., Kashgarian M., Mc Aninch J. E., Proctor I. D., Southon J. R. and Vogel J. S. (1997) The LLNL AMS facility. *Nucl. Instrum. Meth. B.* **123,** 57–61.
Rosenfeld A. H., Barbaro-Galtieri A., Podolsky W. J., Price L. R., Soding P., Wohl C. G., Roos M. and Willis W. J. (1967) Data on particles and resonant states. *Rev. Mod. Phys.* **39,** 1–51.
Rozanski K., Araguas-Araguas L. and Gonfiantini R. (1993) Isotopic patterns in modern global precipitation. In *Climate Change in Continental Isotopic Records, Geophysical Monograph Series* (eds. P. K. Swart, K. C. Lohmann, J. McKenzie and S. Savin). Vol. 78, pp. 1–36. American Geophysical Union, Washington, DC.
Rudolph J., Rath H. K. and Sonntag C. (1984) Noble gases and stable isotopes in ^{14}C-dated palaeowaters from Central Europa and the Sahara. In *Isotope Hydrology 1983,* pp. 467–477. IAEA, Vienna.
Schlosser P., Stute M., Dörr C., Sonntag C. and Münnich K. O. (1988) Tritium/^{3}He-dating of shallow groundwater. *Earth Planet. Sci. Lett.* **89,** 353–362.
Smith G. D., Newhall F., Robinson L. H. and Swanson D. (1964) *Soil temperature regimes: Their characteristics and predictability.* **Report SCS-TP-144,** USDA, Soil Conservation Service.
Solomon D. K., Hunt A. and Poreda R. J. (1996) Source of radiogenic helium 4 in shallow aquifers: Implications for dating young groundwater. *Water Resour. Res.* **32,** 1805–1813.
Stute M. and Sonntag C. (1992) Paleotemperatures derived from noble gases dissolved in groundwater and in relation to soil temperature. In *Isotopes of noble gases as tracers in environmental studies,* pp. 111–122. IAEA, Vienna.
Stute M. and Schlosser P. (1993) Principles and applications of the noble gas paleothermometer. In *Climate Change in Continental Isotopic Records, Geophysical Monograph Series,* (eds. P. K. Swart, K. C. Lohmann, J. McKenzie and S. Savin). Vol. 78, pp. 89–100. American Geophysical Union, Washington, DC.
Stute M. and Schlosser P. (2000). Atmospheric noble gases. In *Environmental tracers in subsurface hydrology* (eds. Vol. P. Cook and A. L. Herczeg) pp. 349–377. Kluwer Academic Publishers, Boston.
Stute M., Schlosser P., Clark J. F. and Broecker W. S. (1992a) Paleotemperatures in the Southwestern United States derived from noble gases in ground water. *Science.* **256,** 1000–1003.
Stute M., Sonntag C., Déak J. and Schlosser P. (1992b) Helium in deep circulating groundwater in the Great Hungarian Plain: Flow dynamics and crustal and mantle helium fluxes. *Geochim. Cosmochim. Acta.* **56,** 2051–2067.
Stute M., Clark J. F., Schlosser P. and Broecker W. S. (1995a) A 30,000 yr continental paleotemperature record derived from noble gases dissolved in groundwater from the San Juan Basin, New Mexico. *Quat. Res.* **43,** 209–220.
Stute M., Forster M., Frischkorn H., Serejo A., Clark J. F., Schlosser P., Broecker W. S. and Bonani G. (1995b) Cooling of tropical Brazil (5 °C) during the Last Glacial Maximum. *Science.* **269,** 379–383.
Tamers M. A. (1975) Validity of radiocarbon dates on ground water. *Geophysical Surveys.* **2,** 217–239.
Thompson L. G., Mosley-Thompson E., Davis M. E., Lin P.-N.,

Henderson K. A., Cole-Dai J., Bolzan J. F. and Liu K.-b. (1995) Late glacial stage and holocene tropical ice core records from Huascarán, Peru. *Science.* **269,** 46–50.

Torgersen T. and Clarke W. B. (1985) Helium accumulation in groundwater, I: An evaluation of sources and the continental flux of crustal ^{4}He in the Great Artesian Basin, Australia. *Geochim. Cosmochim. Acta.* **49,** 1211–1218.

Torgersen T. and Ivey G. N. (1985) Helium accumulation in groundwater, II: A model for the accumulation of the crustal ^{4}He degassing flux. *Geochim. Cosmochim. Acta.* **49,** 2445–2452.

Webb III T., Anderson K. H., Bartlein P. J. and Webb R. S. (1998) Late Quaternary climate change in Eastern North America: A comparison of pollen-derived estimates with climate model results. *Quat. Sci. Rev.* **17,** 587–606.

Weiss R. F. (1968) Piggyback samplers for dissolved gas studies on sealed water samples. *Deep-Sea Res.* **15,** 695–699.

Weiss R. F. (1970) The solubility of nitrogen, oxygen and argon in water and seawater. *Deep-Sea Res.* **17,** 721–735.

Weiss R. F. (1971) Solubility of helium and neon in water and seawater. *J. Chem. Eng. Data.* **16,** 235–241.

Weiss R. F. and Kyser T. K. (1978) Solubility of krypton in water and seawater. *J. Chem. Eng. Data.* **23,** 69–72.

Wigley T. M. L., Plummer L. N. and Pearson F. J. (1978) Mass transfer and carbon isotope evolution in natural water systems. *Geochim. Cosmochim. Acta.* **42,** 1117–1139.

Wilson J. M. and Fleck W. B. (1990) Geology and hydrologic assessment of coastal plain aquifers in the Waldorf area, Charles County, Maryland. Report of Investigations No. 53, Maryland Geological Survey.

Zheng Y. (1999) The marine geochemistry of germanium, molybdenum and uranium: The Sinks. Ph. D. thesis, Columbia University, New York.